

High-precision measurements of $n = 2 \rightarrow n = 1$ transition energies and level widths in He- and Be-like argon ions

J. Machado,^{1,2} C. I. Szabo,^{3,4} J. P. Santos,^{1,*} P. Amaro,¹ M. Guerra,¹ A. Gumberidze,⁵ Guojie Bian,^{2,6} J. M. Isac,² and P. Indelicato^{2,†}

¹Laboratório de Instrumentação, Engenharia Biomédica e Física da Radiação (LIBPhys-UNL), Departamento de Física, Faculdade de Ciências e Tecnologia, FCT, Universidade Nova de Lisboa, P-2829-516 Caparica, Portugal

²Laboratoire Kastler Brossel, Sorbonne Université, CNRS, ENS-PSL Research University, Collège de France, Case 74; 4, Place Jussieu, F-75005 Paris, France

³National Institute of Standards and Technology, Gaithersburg, Maryland 20899, USA

⁴Theiss Research, La Jolla, California 92037, USA

⁵ExtreMe Matter Institute EMMI and Research Division, GSI Helmholtzzentrum für Schwerionenforschung, D-64291 Darmstadt, Germany

⁶Institute of Atomic and Molecular Physics, Sichuan University, Chengdu 610065, People's Republic of China



(Received 5 July 2017; published 26 March 2018)

We performed a reference-free measurement of the transition energies of the $1s2p^1P_1 \rightarrow 1s^2^1S_0$ line in He-like argon, and of the $1s2s^22p^1P_1 \rightarrow 1s^22s^2^1S_0$ line in Be-like argon ions. The highly charged ions were produced in the plasma of an electron-cyclotron resonance ion source. Both energy measurements were performed with an accuracy better than 3 parts in 10^6 , using a double flat-crystal spectrometer, without reference to any theoretical or experimental energy. The $1s2s^22p^1P_1 \rightarrow 1s^22s^2^1S_0$ transition measurement is the first reference-free measurement for this core-excited transition. The $1s2p^1P_1 \rightarrow 1s^2^1S_0$ transition measurement confirms recent measurement performed at the Heidelberg electron-beam ion trap. The width measurement in the He-like transition provides test of a purely radiative decay calculation. In the case of the Be-like argon transition, the width results from the sum of a radiative channel and three main Auger channels. We also performed multiconfiguration Dirac-Fock calculations of transition energies and rates and have done an extensive comparison with theory and other experimental data. For both measurements reported here, we find agreement with the most recent theoretical calculations within the combined theoretical and experimental uncertainties.

DOI: [10.1103/PhysRevA.97.032517](https://doi.org/10.1103/PhysRevA.97.032517)

I. INTRODUCTION

Bound-state quantum electrodynamics (BSQED) and the relativistic many-body problem have been undergoing important progress in the past few years. Yet there are several issues that require increasing the number of high-precision tests. High-precision measurements of transition energies on medium to high- Z elements [1–9], Landé g factors [10–16], and hyperfine structure [17–29], just to name a few, are needed either to improve our understanding or to provide tests of higher-order quantum electrodynamics (QED) corrections, the calculations of which are very demanding.

Recent measurement of the proton size in muonic hydrogen [30,31] and of the deuteron in muonic deuterium [32], which disagree by 7 and 3.5 standard deviations, respectively, from measurements in their electronic counterparts triggered experimental and theoretical research regarding not only the specific issue of the proton and deuteron size, but also the possible anomalies in BSQED. A discrepancy of this magnitude corresponds to a difference in the muonic hydrogen energy of 0.42 meV, which is far outside the calculation uncertainty of about ± 0.01 meV and is much larger than what

can be expected from any omitted QED contribution. Another large discrepancy of 7 standard deviations between theory and experiment has also been observed recently in a specific difference between the hyperfine structures of hydrogenlike and lithiumlike bismuth measured at the experimental storage ring (ESR) at GSI in Darmstadt [29], designed to eliminate the effect of the nuclear magnetization distribution (the Bohr-Weisskopf correction) [22].

Medium and high- Z few-electron ions with a K hole are the object of the present work. They have been studied first in laser-produced plasmas [33] and beam-foil spectroscopy (see, e.g., [34,35]), low-inductance vacuum spark [36], or by using the interaction of fast ion beams with gas targets in heavy-ion accelerators. Ion storage rings have also been used (see, e.g., [37–39]). The limitation in precision of those measurements is mostly due to the large Doppler effect, which affects energy measurements, and the Doppler broadening, which affects any possible width measurement.

Recoil ion spectroscopy [40], which has also been used, is not affected by the Doppler effect, and provides an interesting check. Plasma machines, such as tokamaks, have also provided spectra [41,42], leading to relative measurements, without Doppler shift, usually using He-like lines as a reference. Solar measurements [43] have also been reported.

Accurate transition energy measurements in medium and high- Z , few-electron ions have been reported using either

*jps@fct.unl.pt

†paul.indelicato@lkb.upmc.fr

an electron beam ion trap (EBIT) or electron-cyclotron ion sources (ECRISs) to produce ions at rest in the laboratory. Such measurements, using an EBIT, have been performed by the Livermore group (see, e.g., [8,44–47] and references therein), the Heidelberg group [1,4,9,48], and the Melbourne and National Institute of Standards and Technology (NIST) collaboration [3,5,6]. The present collaboration has reported values using an ECRIS [2].

The Heidelberg group reported the measurement of the $1s2p\ ^1P_1 \rightarrow 1s^2\ ^1S_0$ He-like argon line with a relative accuracy of 1.5×10^{-6} without the use of a reference line [48]. In that work, the spectrometer used is made of a single flat Bragg crystal coupled to a charge-coupled device (CCD) camera, which can be positioned very accurately with a laser beam reflected by the same crystal as the x rays [48]. The Melbourne-NIST collaboration reported the measurement of all the $n = 2 \rightarrow n = 1$ transitions in He-like titanium with a relative accuracy of 15×10^{-6} , using a calibration based on neutral x-ray lines emitted from an electron fluorescence x-ray source [3,5,6]. The Livermore group reported a measurement of all $n = 2 \rightarrow n = 1$ lines in heliumlike copper [8], using hydrogenlike lines in argon as calibration. It also reported measurement of all four lines in He-like xenon, using a microcalorimeter and calibration with x-ray standards [49]. It should be emphasized that measurements in both types of ion sources do not require Doppler shift correction to transition energy measurements, because the ions have only thermal motion.

Measurements of the $1s2s^22p\ ^1P_1 \rightarrow 1s^22s^2\ ^1S_0$ line in Be-like ions are scarce. Some measurements are relative measurements using tokamaks, where the Be-like line appears as a satellite line for the He-like $2 \rightarrow 1$ transitions. The $1s2p\ ^1P_1 \rightarrow 1s^2\ ^1S_0$ line is often used as a calibration. Measurements of that type for Be-like Ar have been performed at the Tokamak de Fontenay aux Roses (TFR) [50], and for Ni at the Tokamak Fusion Test Reactor (TFTR) [41,42]. Such relative measurements, which use theoretical results on the He-like line, must be recalibrated using the most recent theoretical values. Several other observations have been made on different elements, but no experimental energy reported (see, e.g., Ref. [51] for Cl, Ar, and Ca), or the experimental accuracy is not completely documented (see, e.g., [52–54]). Measurements in EBIT are also known, as in vanadium [55] and iron [56], for terrestrial and astrophysics plasma applications. There have also been relative measurements in ECRIS for sulfur, chlorine, and argon [57], using the relativistic M1 transition $1s2s\ ^3S_1 \rightarrow 1s^2\ ^1S_0$ as a reference.

Chantler *et al.* [3,5,58], have claimed that existing data show the evidence of a discrepancy between the most advanced BSQED calculation [59] and measurements in the He-like isoelectronic sequence, leading to a deviation that scales as $\approx Z^3$. They speculated [5] that this supposed systematic effect could provide insight into the *proton size puzzle*, the Rydberg and fine-structure constants, or missing three-body BSQED terms. Here we make a detailed analysis, including all available experimental results, to check this claim.

We emphasize the advantage of studying highly charged, medium- Z systems, such as argon ions, to test QED. The BSQED contributions have a strong Z dependence: The retardation correction to the electron-electron interaction contribution scales as Z^3 , and the one-electron corrections, self-energy

and vacuum polarization, scale as Z^4 . Yet, at high Z , the strong enhancement of the nuclear size contribution and associated uncertainty limits the degree to which available experimental measurements can be used to test QED [58,60–63]. At very low Z , experiments can be much more accurate, but tests of QED can be limited as well, even for very accurate measurements of transitions to the ground state of He [64–66]. For few-electron atoms and ions, they are limited by the large size of electron-electron correlation and by the evaluation of the needed higher-order QED screening corrections, in the nonrelativistic QED formalism (NRQED) [67–71]. It can also be limited by the slow convergence of all-order QED contributions at low Z , which may be required for comparison, and because of the insufficient knowledge of some nuclear parameters, namely the form factors and polarizability [30–32,59]. In medium- Z elements like argon or iron, the nuclear mean spherical radii are sufficiently well known (see, e.g., [72]) and nuclear polarization contribution to the ion level energies is very small. So uncertainties related to the nucleus are small compared to experimental and theoretical accuracy. This can be seen in the theoretical uncertainties claimed in Ref. [59].

Besides the fundamental aspect, knowledge of transition energies and wavelengths of highly charged ions is very important for many sectors of research, such as astrophysics or plasma physics. For example, an unidentified line was recently detected in the energy range 3.55–3.57(3) keV in an x-ray multimirror (XMM-Newton) space x-ray telescope spectrum of 73 galaxy clusters [73] and at 3.52(3) keV for another XMM spectrum in the Andromeda galaxy and the Perseus galaxy cluster [74]. The next year a line at 3.53(11) keV was observed in the deep exposure data set of the Galactic Center region with the same instrument. A possible connection with a dark matter decay line has been put forward, yet measurements performed with an EBIT seem to show that it could be a set of lines in highly charged sulfur ions, induced by charge exchange [75], while a recently published search with the high-resolution x-ray spectrometer of the HITOMI satellite does not find evidence for such lines in the Perseus cluster [76].

In the present work, we apply the method we have developed to measure the energy and linewidth of the $1s2s\ ^3S_1 \rightarrow 1s^2\ ^1S_0$ M1 transition reported in Ref. [2], to the $1s2p\ ^1P_1 \rightarrow 1s^2\ ^1S_0$ transition in He-like argon and to the $1s^22s2p\ ^1P_1 \rightarrow 1s^22s^2\ ^1S_0$ transition in Be-like argon ions. We also present a multiconfiguration Dirac-Fock (MCDF) calculation for the two transition energies and widths. These calculations are performed with a new version of the MCDGME code that uses the effective operators developed by the St. Petersburg group to evaluate the self-energy screening [77].

The article is organized as follows. In the next section we briefly describe the experimental setup used in this work. A detailed description of the analysis method that provides the energy, width, and uncertainties is given in Sec. III. A brief description of the calculations of transition energy and widths is given in Sec. IV. We present our experimental result for the $1s2p\ ^1P_1 \rightarrow 1s^2\ ^1S_0$ transition in Sec. V. In the same section we present all available experimental results for $7 \leq Z \leq 92$ and $n = 2 \rightarrow n = 1$ transitions in He-like ions. We do a very detailed comparison between theory from Ref. [59], which covers $12 \leq Z \leq 92$ and the available measurements in this Z range. Our results and comparison with theory for

the $1s2s^2 2p^1 P_1 \rightarrow 1s^2 2s^2 1S_0$ line in Be-like argon ions are presented in Sec. VI. The conclusions are provided in Sec. VII.

II. EXPERIMENTAL METHOD

ECRIS plasmas have been shown to be very intense sources of x rays, and have diameters of a few centimeters. Therefore, they are better adapted to spectrometers that can use an extended source. At low energies one can thus use cylindrically or spherically bent crystal spectrometers as well as double-crystal spectrometers (DCSs).

A single flat-crystal spectrometer, combined with an accurate positioning of the detector, and alternate measurements, symmetrical with respect to the optical axis of the instrument, as used in Heidelberg [48], and the double-crystal spectrometers [78,79] are the only two methods that can provide high-accuracy, reference-free measurements in the x-ray domain. We use here *reference free* with the same meaning as in Ref. [80], i.e., the measured wavelengths are directly connected to the meter as defined in the International System of Units, through the lattice spacing of the crystals [79]. Our group reported in 2012 such a measurement of the $1s2s^3 S_1 \rightarrow 1s^2 1S_0$ transition energy in He-like argon with an uncertainty of 2.5×10^{-6} without the use of an external reference [2], using the same experimental device as in the present work: a DCS connected to an ECRIS, the ‘‘Source d’ Ions Multichargés de Paris’’ (SIMPA) [81], jointly operated by the Laboratoire Kastler Brossel and the Institute des Nanosciences de Paris on the Université Pierre and Marie Curie campus.

A detailed description of the experimental setup of the DCS at the SIMPA ECRIS used in this work is given in Ref. [79]. A neutral gas (Ar in the present study) is injected into the plasma chamber inside a magnetic system with minimum fields at the very center of the vacuum chamber. Microwaves at a frequency of 14.5 GHz heat the electrons that are trapped by the magnetic field. The energetic electrons ionize the gas through repeated collisions reaching up to heliumlike charge states [82]. The ions are, in turn, trapped by the space charge of the electrons, which have a density around $1 \times 10^{11} \text{ cm}^{-3}$. This corresponds to a trapping potential of a fraction of 1 V, leading to an ion-speed distribution of ≈ 1 eV per charge, and thus to a small Doppler broadening of all the observed lines. In contrast, EBITs have a trapping potential of several hundred eV, and the Doppler broadening is then much larger.

The $1s2s^3 S_1$ state is mostly created by electron ionization of the $1s^2 2s^2 S_{1/2}$ ground state of Li-like argon, and therefore the $1s2s^3 S_1 \rightarrow 1s^2 1S_0$ line is the most intense line we observed in He-like argon. The $1s2p^1 P_1 \rightarrow 1s^2 1S_0$ line observed here results from the excitation of the $1s^2 1S_0$ He-like argon ground state, which is much less abundant, leading to a weaker line. The Be-like excited level, $1s2s^2 2p^1 P_1$, is mostly produced by ionization of the ground state of boronlike argon, which is a well-populated charge state (see Fig. 21, Ref. [79]). The $1s2s^2 2p^1 P_1 \rightarrow 1s^2 2s^2 1S_0$ line is thus the most intense we observed.

The spectra are recorded by a specially designed, reflection vacuum double-crystal spectrometer described in detail in Ref. [79]. The two (6×4) cm^2 , 6 mm-thick Si(111) crystals were made at the National Institute for Standards and Technology (NIST). Their lattice spacing in vacuum was measured and

found to be $d_{111} = 3.135601048(38) \text{ \AA}$ (relative uncertainty of 0.012×10^{-6}) at a temperature of 22.5°C [79], relative to the standard value [83,84]. More details will be found in Ref. [85]. Using this lattice spacing, our measurement provides wavelengths directly tied to the definition of the meter [84]. The DCS is connected to the ion source in such a way that the axis of the spectrometer is aligned with the ECRIS axis and is located at 1.2 m from the plasma (a sphere of ≈ 3 cm in diameter).

To analyze the experimental spectra, we developed a simulation code [79], which uses the geometry of the instrument and of the x-ray source, the shape of the crystal reflectivity profile, as well as the natural Lorentzian shape of the atomic line and its Gaussian Doppler broadening to perform high-precision ray tracing. The reflectivity profile is calculated using the x-ray oriented program (XOP) [86], which uses dynamical diffraction theory from Ref. [87], and the result is checked with the XOH program, which calculates crystal susceptibilities χ_0 and χ_h [88,89].

The first crystal is maintained at a fixed angle. A spectrum is obtained by a series of scans of the second crystal. A stepping motor, driven by a microstepper, runs continuously, between two predetermined angles that define the angular range of one spectrum. X rays are recorded continuously and stored in a histogram, together with both crystal temperatures. Successive spectra are recorded in opposite directions. Both crystal angles are measured with Heidenhain¹ high-precision angular encoders. The experiment is performed in the following way: a nondispersive-mode (NDM) spectrum is recorded first. Then a dispersive-mode (DM) spectrum is recorded. The sequence is completed with the recording of a second NDM spectrum. Due to the low counting rate, such a sequence of three spectra takes a full day to record. In order to obtain enough statistics, the one-day sequence is repeated typically 7–15 times.

III. DATA ANALYSIS

The data analysis is performed in three steps. First we derive a value for the experimental natural width of the line. For this, each experimental dispersive-mode spectrum is fitted with simulated spectra, using an approximate energy (e.g., the theoretical value) and a set of Lorentzian widths. A weighted one-parameter fit is performed on all the results for all recorded dispersive-mode spectra providing a width value and its uncertainty. This experimental width is then used to generate a new set of simulations, using several different energies and crystal temperatures. These simulations are used to fit each dispersive-mode and nondispersive-mode experimental spectrum in order to obtain the line energy. For each day of data recording this leads to two Bragg angle values, obtained by taking the angular difference between a nondispersive-mode spectrum and a dispersive-mode spectrum.

¹Certain commercial equipment, instruments, or materials are identified in this paper to foster understanding. Such identification does not imply recommendation or endorsement by the National Institute of Standards and Technology, nor does it imply that the materials or equipment identified are necessarily the best available for the purpose.

(1) One Bragg angle value is obtained by comparing the first nondispersive-mode spectrum of the day and the dispersive-mode spectrum obtained immediately after.

(2) A second Bragg angle value is obtained by comparing the same dispersive-mode spectrum with the nondispersive-mode spectrum obtained immediately after.

In that way a number of possible time-dependent drifts in the experiment are compensated. We now describe these processes in more detail.

A. Evaluation of the widths

The ion temperature, which is necessary to calculate the Gaussian broadening was obtained by measuring first a line with a completely negligible natural width, the M1 $1s2s^3S_1 \rightarrow 1s^2^1S_0$, transition. The width of this transition is $\approx 1 \times 10^{-7}$ eV, which is totally negligible when compared to our spectrometer inherent energy resolution. From this analysis we obtained the Gaussian broadening $\Gamma_G^{\text{Exp.}} = 80.5(46)$ meV [2]. This value also provides the depth of the trapping potential due to the electron space charge. Knowing the experimental Gaussian broadening value $\Gamma_G^{\text{Exp.}}$, we can perform all the needed simulations. For each line under study we then proceed as follows.

(1) Perform simulations for the dispersive-mode spectra for a set of natural width values Γ_L^i and the theoretical transition energy E_0 , using the already known $\Gamma_G^{\text{Exp.}}$, and crystal temperature $T_{\text{Ref.}} = 22.5^\circ\text{C}$.

(2) Interpolate each simulation result with a piecewise spline function to obtain a set of continuous, parametrized functions $S_{[E_0, \Gamma_L^i, \Gamma_G^{\text{Exp.}}, T]}(\theta - \theta_0)$, where θ_0 correspond to the angle at which the simulation reaches its maximum value, and $T = T_{\text{Ref.}}$.

(3) Normalize all the functions above to have the same maximum value (we chose the one with $\Gamma_L = 0$ as reference).

(4) Fit each experimental spectrum with the functions obtained above,

$$I(\theta - \theta_0, I_{\text{max}}, a, b) = I_{\text{max}} S_{[E_0, \Gamma_L^i, \Gamma_G^{\text{Exp.}}, T]}(\theta - \theta_0) + a + b\theta, \quad (1)$$

where I_{max} is the line intensity, θ the crystal angle, a the background intensity, and b the background slope. The parameters θ_0 , I_{max} , a , and b are adjusted to minimize the reduced $\chi^2(\Gamma_L^i)$. We perform a series of fits of each experimental spectrum, with 27 simulated spectra, each evaluated with a different width Γ_L^i , to obtain a set of $\chi^2(\Gamma_L^i)$ values. The width values go from 0 to 250 meV by steps of 10 meV, completed by a point at 300 meV. A typical experimental spectrum and the fitted simulated functions, for five of the 27 values of Γ_L^i used to make the analysis, are shown in Fig. 1.

(5) Fit a third degree polynomial to the set of points $[\Gamma_L^i, \chi^2(\Gamma_L^i)]$.

(6) Find the minimum of the third degree polynomial to get the corresponding optimal $\Gamma_{L,\text{opt.}}^n$, n being the experiment run number (see Fig. 2 for an example).

(7) Get the 68% error bar $\delta\Gamma_{L,\text{opt.}}^n$ for experiment run n by finding the values of the width for which [90]

$$\chi^2(\Gamma_{L,\text{opt.}}^n \pm \delta\Gamma_{L,\text{opt.}}^n) = \chi^2(\Gamma_{L,\text{opt.}}^n) + 1. \quad (2)$$

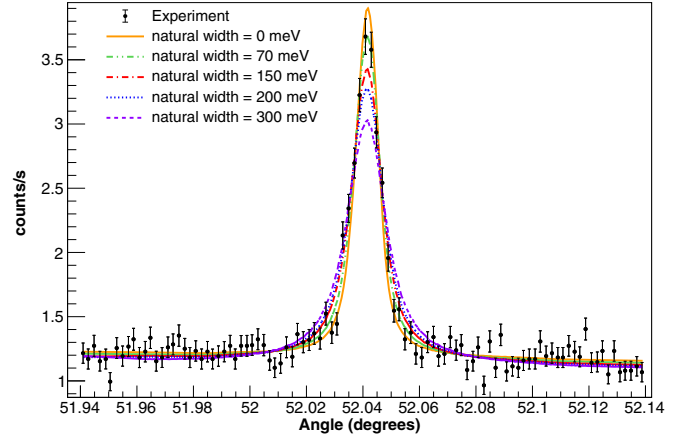


FIG. 1. Example of a dispersive-mode experimental spectrum for the He-like Ar $1s2p^1P_1 \rightarrow 1s^2^1S_0$ transition (black dots), together with a few plots of the function in Eq. (1), for different values of the natural line width Γ_L^i . The four parameters have been adjusted to minimize the reduced $\chi^2(\Gamma_L)$ (see text for more explanations).

(8) Finally a weighted average of the values in the set of all the $\Gamma_{L,\text{opt.}}^n$ obtained for all measured spectra is performed to obtain the experimental value $\Gamma_L^{\text{Exp.}}$ and its error bar:

$$\frac{1}{(\delta\Gamma_L^{\text{Exp.}})^2} = \sum_n \frac{1}{(\delta\Gamma_{L,\text{opt.}}^n)^2},$$

$$\Gamma_L^{\text{Exp.}} = (\delta\Gamma_L^{\text{Exp.}})^2 \sum_n \frac{\Gamma_{L,\text{opt.}}^n}{(\delta\Gamma_{L,\text{opt.}}^n)^2}. \quad (3)$$

The sets of $\Gamma_{L,\text{opt.}}^n$ for both lines studied here are plotted in Fig. 3.

The two first steps are performed by two different methods, one based on the Centre Européen de Recherche Nucléaire (CERN) program ROOT, version 6.08 [91–93], and one based on MATHEMATICA, version 11 [94].

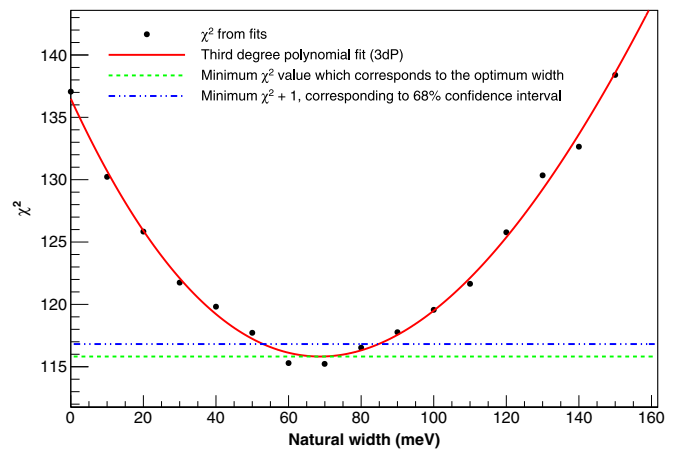


FIG. 2. Third degree polynomial fitted to the $[\Gamma_L, \chi^2(\Gamma_L)]$ set of points (black dots), for the He-like Ar $1s2p^1P_1 \rightarrow 1s^2^1S_0$ transition. The χ^2 values were obtained from the fits, a few of which are represented in Fig. 1, with 27 different values of Γ_L . The blue dashed-dotted line corresponds to Eq. (2).

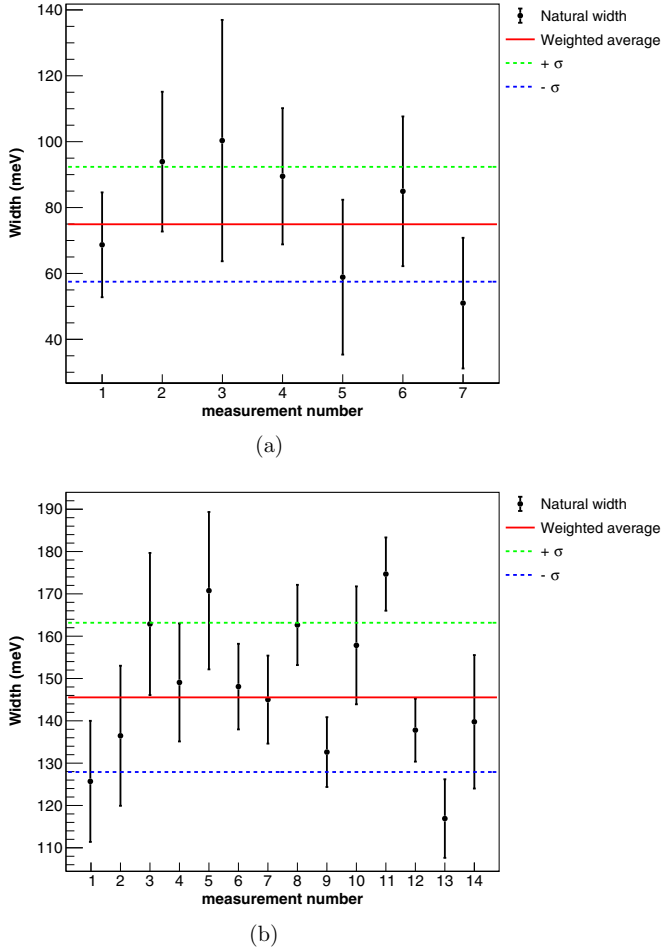


FIG. 3. Natural width values of all the spectra recorded during the experiment, with weighted average and uncertainties evaluated with Eq. (3). (a) He-like argon $1s2p\ ^1P_1 \rightarrow 1s^2\ ^1S_0$ transition. (b) Be-like argon $1s2s^2 2p\ ^1P_1 \rightarrow 1s^2 2s^2\ ^1S_0$ transition.

B. Transition energy values

Once we obtained the experimental width value $\Gamma_L^{\text{Exp.}}$ of a measured line (cf. Sec. III A), the determination of the correspondent experimental transition energy value E_{Exp} is achieved using the following scheme.

(1) Perform simulations in the nondispersive and dispersive modes for a set of transition energy values $E_k = E_{\text{theo}} + k\Delta E$, where E_{theo} is the theoretical energy value, ΔE an energy increment, and k an integer that can take positive or negative values. The simulations are done with the experimental natural width $\Gamma_L^{\text{Exp.}}$ and Gaussian broadening $\Gamma_G^{\text{Exp.}}$. The simulations are performed at various crystal temperature values T_l for each energy.

(2) As in Sec. III A, interpolate each simulation result with a spline function for both the nondispersive and dispersive modes, to obtain a set of functions depending on all the (E_k, T_l) pairs.

(3) Fit each experimental spectrum, using Eq. (1) with $E_0 = E_k$ and $T = T_l$, to obtain the angle difference between the simulation and the experimental spectrum, both in dispersive and nondispersive modes.

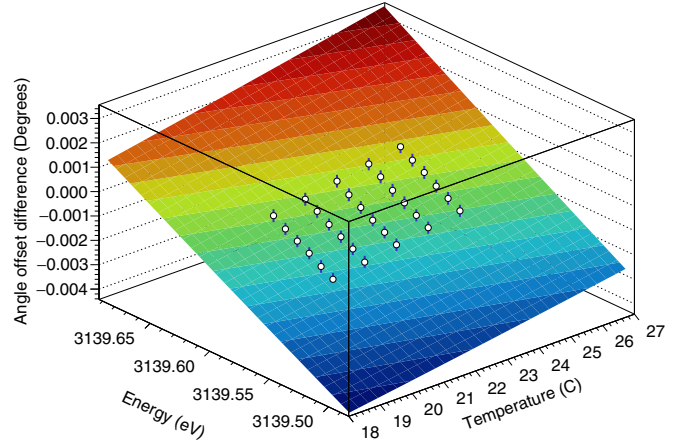


FIG. 4. Fitted two-dimensional function from Eq. (4), and experimental results (white spheres), for the He-like Ar $1s2p\ ^1P_1 \rightarrow 1s^2\ ^1S_0$ transition. The fit is performed taking into account the statistical error bars in each point.

(4) For each pair of dispersive- and nondispersive-mode experimental spectra, calculate the offsets $\Delta\theta_{\text{Exp.}-\text{Simul.}}^{n,k,l} = (\theta_{\text{Exp.},\text{DM}}^n - \theta_{\text{Exp.},\text{NDM}}^n) - (\theta_{\text{Simul.},\text{DM}}^{k,l} - \theta_{\text{Simul.},\text{NDM}}^{k,l})$ between the simulated spectra and the experimental value obtained in the step above. This offset should be 0 if the energy and temperature used in the simulation were identical to the experimental values.

(5) Fit the bidimensional function,

$$\Delta\theta_{\text{Exp.}-\text{Simul.}}(E, T) = p + qE + rE^2 + sET + uT + vT^2, \quad (4)$$

where $p, q, r, s, u,$ and v are adjustable parameters, to the set of points $[E_k, T_l, \Delta\theta_{\text{Exp.}-\text{Simul.}}^{n,k,l}]$ obtained in the previous step (see Fig. 4 as an example).

(6) The experimental line energy $E_{\text{Exp.}}^n$ for spectrum pair number n , is the energy such that $\Delta\theta_{\text{Exp.}-\text{Simul.}}(E_{\text{Exp.}}^n, T_{\text{Exp.}}) = 0$ where $T_{\text{Exp.}}$ stands for the average measured temperature on the second crystal.

(7) As a check, we also used the line energy such that $\Delta\theta_{\text{Exp.}-\text{Simul.}}(E_{\text{Exp.}}^n, T_{\text{Ref.}}) = 0$ ($T_{\text{Ref.}} = 22.5^\circ\text{C}$). This leads to a temperature-dependent energy. We then fitted a straight line to the line energy, as a function of the second crystal temperature, and extrapolated to $T = 22.5^\circ\text{C}$. Both methods lead to very close values, well within the uncertainties.

(8) As in Sec. III A, we calculate the weighted average of all the $(n, E_{\text{Exp.}}^n)$ pairs to obtain the final experimental energy. The error bar on each point is the quadratic combination of the instrumental uncertainty, as given in Table I, and of the statistical error.

(9) To check the result, we also fit the set of $(E_{\text{Exp.}}^n, T_{\text{Exp.}}^n)$ pairs with the function $E_0 + bT$ to check that there is no residual temperature dependence.

IV. THEORETICAL CALCULATION

The core-excited $1s2s^2 2p\ ^1P_1 \rightarrow 1s^2 2s^2\ ^1S_0$ transition in Be-like ions has been calculated with the most recent methods, only very recently and only for iron [95] and argon [96].

TABLE I. Instrumental contributions to the uncertainties in the analysis of the daily experiments (see Refs. [2,79]).

Contribution	Value (eV)
Crystal tilts ($\pm 0.01^\circ$ for each crystal)	0.0002
Vertical misalignment of collimators (1 mm)	0.0002
X-ray source size (6–12 mm)	0.0013
Form factors	0.0020
X-ray polarization	0.0014
Angle encoder error	0.0036
Lattice spacing error	0.00012
Index of refraction	0.0016
Coefficient of thermal expansion	0.00019
X-ray polarization	0.00100
Energy-wavelength correction	0.000078
Temperature (0.5°C)	0.0040

Previous calculations [97–100] did not take into account QED and relativistic effects to the extent possible today.

For the preparation of this experiment, we performed a calculation of the energy value for the $1s2s^22p^1P_1 \rightarrow 1s^22s^2^1S_0$ transition in Be-like argon, using the multiconfiguration Dirac-Fock approach as implemented in the 2017.2 version of the relativistic MCDF code (MCDGME), developed by Desclaux and Indelicato [101–104]. The full description of the method and the code can be obtained from Refs. [101,105–107]. The present version also takes into account the normal and specific mass shifts, evaluated following the method of Shabaev [108–110], as described in [111,112].

The main advantage of the MCDF approach is the ability to include a large amount of electronic correlation by taking into account a limited number of configurations [113–115]. All calculations were done for a finite nucleus using a uniformly charged sphere. The atomic masses and the nuclear radii were taken from the tables by Audi *et al.* [116] and Angeli and Marinova [72,117], respectively.

Radiative corrections are introduced from a full QED treatment. The one-electron self-energy is evaluated using the one-electron values of Mohr and co-workers [118–122], and corrected for finite nuclear size [123]. The self-energy screening and vacuum polarization were included using the methods developed by Indelicato and co-workers [102,103,124–126].

TABLE II. Total energy and transition energies (in eV) for the $1s2s^22p^1P_1 \rightarrow 1s^22s^2^1S_0$ transition in Be-like argon, as a function of the maximum principal quantum number n of the correlation orbitals. All correlation from the Coulomb, retardation, and QED parts is included. Extrapolation for $n \rightarrow \infty$ is done by fitting the function $a + b/n^2 + c/n^3$ to the correlation energy [difference with the energy for n and the Dirac-Fock (DF) value] of each level and retaining only the constant term a . The uncertainty combines the difference between the extrapolated and best directly calculated value, the missing Auger shift, and the self-energy screening model.

n	Welton QED			Model operator QED [77,127]		
	Initial	Final	Transition	Initial	Final	Transition
DF	−7222.7485	−10313.5817	3090.8333	−7222.7522	−10319.3215	3096.5692
2	−7227.3514	−10319.3250	3091.9736	−7227.3551	−10319.3320	3091.9769
3	−7228.6879	−10320.5341	3091.8462	−7228.6915	−10320.5417	3091.8502
4	−7229.0470	−10320.7556	3091.7086	−7229.0506	−10320.7638	3091.7131
5	−7229.1988	−10320.8783	3091.6795	−7229.2024	−10320.8870	3091.6846
∞	−7229.4027	−10321.1125	3091.7098	−7229.4064	−10321.1225	3091.7161

In previous work, the self-energy screening in this code was based on the Welton approximation [102,103]. Here we also evaluate the self-energy screening following the model operator approach recently developed by Shabaev *et al.* [77,127], which has been added to MCDGME. A detailed description of this new code will be given elsewhere.

In order to assess the quality of this new method for calculating the self-energy screening we can compare the different values for the He-like transition measured here. The QED value of Indelicato and Mohr [128] is 0.1100 eV, and the one from Ref. [59] (Table IV) is 0.1085. The Welton method provides 0.0916 eV, while the implementation of the St. Petersburg effective operator method gives 0.0965 eV, closer to the *ab initio* methods. We can thus assume an uncertainty of 0.014 eV and 0.018 eV for the effective operator and Welton operator methods, respectively. The same procedure applied to the Be-like transitions provides 0.130 eV using Ref. [128], 0.112 eV for the effective operator method and 0.109 eV for the Welton method. We can conclude that at intermediate Z , both the Welton and effective operator methods provide very similar results, the effective operator method being in slightly better agreement with *ab initio* calculation. This is consistent with earlier comparisons for fine-structure transitions (see, e.g., Ref. [129]).

Lifetime evaluations are done using the method described in Ref. [130]. The orbitals contributing to the wave function were fully relaxed, and the resulting nonorthogonality between initial and final wave functions fully taken into account, following [131,132].

The full Breit interaction and the Uehling potential are included in the self-consistent field process. Projection operators have been included [107] to avoid coupling with the negative energy continuum.

As a check, we also performed a calculation of the He-like argon lines measured in the present work and in Ref. [2]. Following Refs. [107,133–135], we use for the excited state the following configurations:

$$\begin{aligned}
|1s2p^1P_1\rangle = & c_1|1s2p, J=1\rangle + c_2|2s3p, J=1\rangle \\
& + c_3|2p'3d, J=1\rangle + c_4|3s4p, J=1\rangle \\
& + c_5|3p'4d, J=1\rangle + c_6|3d'4f, J=1\rangle \\
& + c_7|4s5p, J=1\rangle + c_8|4p'5d, J=1\rangle \\
& + c_9|4d'5f, J=1\rangle + c_{10}|4f'5g, J=1\rangle
\end{aligned}$$

TABLE III. Convergence of theoretical partial radiative widths, Auger widths, and energies for transitions originating from the Be-like $1s2s^22p^1P_1$ level. Transition energies are in eV and widths in meV.

Max. n	Radiative		Auger						Total width
	$\rightarrow 1s^22s^2^1S_0$		$\rightarrow 1s^22s^2S_{1/2}$		$\rightarrow 1s^22p^2P_{1/2}$		$\rightarrow 1s^22p^2P_{3/2}$		
	Energy	Width	Energy	Width	Energy	Width	Energy	Width	
DF	3096.57	62.79	2240.96	0.52	2208.96	14.36	2205.80	48.87	126.54
2	3091.98	64.58	2237.06	24.34	2205.22	3.64	2201.85	8.83	101.39
3	3091.85	63.43	2236.33	1.29	2204.44	2.24	2201.23	6.30	73.26
4	3091.71	63.11	2236.12	0.22	2204.24	16.13	2201.06	49.29	128.75
5	3091.68	63.12	2235.99	0.29	2204.14	2.34		NC	

$$\begin{aligned}
& + c_{11}|5s6p, J=1\rangle + c_{12}|5p'6d, J=1\rangle \\
& + c_{13}|5d'6f, J=1\rangle + c_{14}|5f'6g, J=1\rangle \\
& + c_{15}|5g'6h, J=1\rangle, \quad (5)
\end{aligned}$$

where the l' indicates an orbital with identical angular function as the l one, but with another radial wave function, for which the orthogonality with orbitals of the same symmetry in another configuration is not enforced. The ground-state wave function is taken as usual as $|1s^2^1S_0\rangle = c_1|1s^2, J=0\rangle + c_2|2s^2, J=0\rangle + c_3|2p^2, J=0\rangle + \dots + c_{20}|6g^2, J=0\rangle + c_{21}|6h^2, J=0\rangle$. We also evaluated

$$\begin{aligned}
|1s2s^3S_1\rangle = & c_1|1s2s, J=1\rangle + c_2|2p3p, J=1\rangle \\
& + c_3|3s4s, J=1\rangle + c_4|3d4d, J=1\rangle \\
& + c_5|4p5p, J=1\rangle + c_6|4f5f, J=1\rangle \\
& + c_7|5s6s, J=1\rangle + c_8|5d6d, J=1\rangle \\
& + c_9|5g6g, J=1\rangle, \quad (6)
\end{aligned}$$

in order to calculate the M1 transition energies measured in Ref. [2], which allowed one to compare also energy differences.

TABLE IV. Comparison between theoretical partial radiative widths, Auger widths, and energies for transitions originating from the Be-like $1s2s^22p^1P_1$ level. Transition energies are in eV and widths in meV.

Initial level	Final level	MCDF, Chen (1985) [99]		MCDF, Costa <i>et al.</i> (2001) [139]		RCI, Natarajan (2003) [140]	
		Energy	Rate	Energy	Rate	Energy	Rate
$1s2s^22p^1P_1$	$1s^22s^2^1S_0$	3090.66	66.48	3091.95	64.57	3088.958	64.58
$1s2s^22p^1P_1$	$1s^22s_{1/2}$	2236.81		2237.03	18.76		
	$1s^22p_{1/2}$	2204.79		2205.19	15.01		
	$1s^22p_{3/2}$	2201.63		2201.82	52.53		
Total Auger			80.30		86.29		
Level width			146.78		150.86		
		MCDF (this work)		FAC (this work)			
		Energy	Rate	Energy	Rate		
$1s2s^22p^1P_1$	$1s^22s^2^1S_0$	3091.72	63.12	3091.11	63.48		
$1s2s^22p^1P_1$	$1s^22s_{1/2}$	2235.99	0.29	2241.39	1.13		
	$1s^22p_{1/2}$	2204.14	2.34	2209.22	12.93		
	$1s^22p_{3/2}$	2201.06	49.31	2206.10	43.82		
Total Auger			51.94		57.89		
Level width			128 (40)		121.36		

For Be-like argon, the correlation contributions result from the inclusion of all single, double, and triple electron excitations of the $n=1$ and 2 electrons in the unperturbed configuration up to $n=5$. For the $1s^22s^2^1S_0$ ground state it corresponds to 2478 configurations and for the $1s2s^22p^1P_1$ excited state to 14 929 configurations. We performed an estimation of the full correlation energy by doing a fit with the function $a + b/n^2 + c/n^3$, and extrapolation to $n \rightarrow \infty$ for each level, for both the Welton and the Model operator values. The results are presented in Table II. By comparing the extrapolated value and the changes in QED due to the use of either the Welton or effective operator method we estimated the theoretical uncertainty provided in the table. There is, however, a contribution that is not included, the Auger shift. This shift is due to the fact that the $1s2s^22p^1P_1$ being core excited is degenerate with a continuum. To our knowledge, such shifts have been evaluated only in the case of neutral atom x-ray spectra [124,125,136]. For argon with a $1s$ hole, the shift is 165 meV, while for a $2p$ hole it is 11 meV. Here we have a four-electron system, with only three possible Auger channels, and the $2s$ shell is closed, so the effect is expected to be small. We assume an extra theoretical uncertainty of 11 meV for this uncalculated term.

TABLE V. Measured and computed natural line width values for the $1s2p\ ^1P_1 \rightarrow 1s^2\ ^1S_0$ transitions in He-like Ar. All values are given in meV, and estimated uncertainties are shown in parentheses.

Transition	Experiment	Theory	Reference
$1s2p\ ^1P_1 \rightarrow 1s^2\ ^1S_0$	75 (17)	70.4778 (25)	MCDF (this work)
		70.40	MBPT, Si <i>et al.</i> (2016) [145]
		70.43	MCDHF, Si <i>et al.</i> (2016) [145]
		70.43	Johnson <i>et al.</i> (1995) [142]
		70.49 (14)	Drake (1979) [141]

The Auger width of the $1s2s^22p\ ^1P_1$ level is calculated with the MCDFGME code, following the method described in Ref. [137] with full relaxation and final-state channel mixing, again taking into account the nonorthogonality between the initial and final state. For the first time, we combine this method with fully correlated wave functions, up to $n = 5$. The convergence of the transition energy and width are presented in Table III. This table shows that the Auger width values vary rather strongly when increasing the maximum n of correlation orbitals, when nonorthogonality and full relaxation are included. This behavior is due to the fact that the free electron wave functions have to be orthogonal to all the occupied and correlation orbitals of the same symmetry, which provides a lot of constraints.

We have also performed calculations of the transition energies and rates with the “flexible atomic code” (FAC), widely used in plasma physics [138]. This code is based on the relativistic configuration interaction (RCI), with independent

particle basis wave functions that are derived from a local central potential. This local potential is derived self-consistently to include the screening of the nuclear potential by the electrons.

The final results are compared to other calculations from Refs. [99,139,140] in Table IV. The relatively large difference between our present MCDF calculation and the Dirac-Fock calculation from Ref. [139], made with an earlier version of our code, is due to correlation and to the evaluation of Auger rates using fully relaxed initial and final states.

The contributions of all the other possible transitions to the $1s^2\ n\ l\ J$ levels, $n = 3 \rightarrow \infty$, were evaluated by computing all Auger widths up to $n = 9, l = 8$. We then fitted a function $a/n^2 + b/n^3$ to the total Auger width for each principal quantum number n , summing all values of L and J for each value of n , to evaluate the contribution from $n = 10$ up to infinity. We find $a = 0.056\ 2325$ meV and $b = 0.530\ 28$ meV. The total value for the contribution of all levels with $n \geq 3$ is 0.063 meV and is thus negligible.

TABLE VI. Comparison of our He-like argon experimental $1s2p\ ^1P_1 \rightarrow 1s^2\ ^1S_0$ transition energy with previous experimental and theoretical values. All energies are given in eV, and estimated uncertainties are shown in parentheses.

Energy	Reference	Expt. method
	Experiment	
3139.5927(50)(63)(80)	This work (stat.)(syst.)(tot.)	ECRIS
3139.567(11)	Schlessner <i>et al.</i> (2013) [57]	ECRIS
3139.581(5)	Kubiček <i>et al.</i> (2012) [48]	EBIT
3139.583(63)	Bruhns <i>et al.</i> (2007) [1]	EBIT
3139.552(37)	Deslattes <i>et al.</i> (1984) [40]	Recoil ions
3139.60(25)	Briand <i>et al.</i> (1983) [35]	Beam-foil
3140.1(7)	Dohmann <i>et al.</i> (1979) [34]	Beam-foil
3138.9(9)	Neupert <i>et al.</i> (1971) [43]	Solar emission
	Theory	
3139.559 (10) (13)	This work using model operators [77,127] (correlation)(SE screening)	
3139.553 (10) (18)	This work using Welton model (correlation)(SE screening)	
3139.538	MBPT, Si <i>et al.</i> (2016) [145]	
3139.449	MCDHF, Si <i>et al.</i> (2016) [145]	
3139.5821 (4)	Artemyev <i>et al.</i> (2005) [59]	
3139.582	Plante <i>et al.</i> (1994) [148]	
3139.617	Cheng <i>et al.</i> (1994) [149]	
3139.576	Drake (1988) [150]	
3139.649	Indelicato <i>et al.</i> (1987) [103]	
3139.56	Safronova (1981) [151]	
3140.15	Johnson <i>et al.</i> (1976) [152]	
3140.46	Gabriel (1972) [153]	

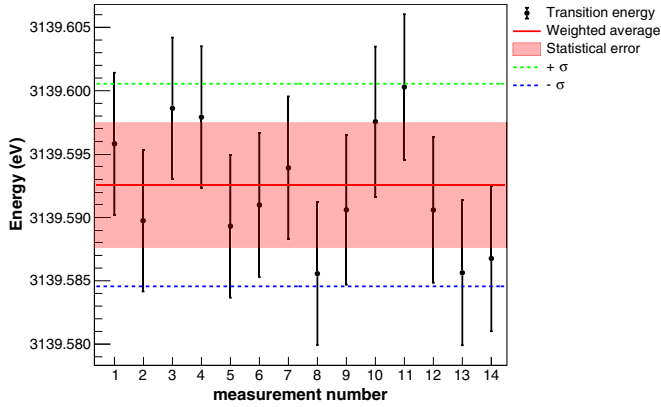


FIG. 5. He-like argon $1s2p\ ^1P_1 \rightarrow 1s^2\ ^1S_0$ transition energy values of the different spectra recorded during the experiment. Error bars in each point correspond to the quadratic sum of the peak fitting uncertainty with the uncertainties from Table I, which have random fluctuations only, i.e., the angle measurement and the temperature correction. The (pink) shaded area corresponds to the weighted average of the peak position statistical uncertainty obtained from the fit. The $\pm 1\sigma$ lines combine these statistical uncertainties with all systematic errors from Table I. Every pair of points corresponds to one-day data taking (see text for explanations).

V. RESULTS AND COMPARISON WITH THEORY FOR THE HE-LIKE $1s2p\ ^1P_1 \rightarrow 1s2s\ ^1S_0$ TRANSITION

A. Line widths

Our experimental values for the line widths, obtained as explained in Sec. III A and Fig. 3(a), are presented in Table V, together with several theoretical results. There are several possible E1 radiative transitions originating from the $1s2p\ ^1P_1$ level. Because of the large energy difference, the contribution of the $1s2p\ ^1P_1 \rightarrow 1s^2\ ^1S_0$ transition to the level width is strongly dominant. The next largest contribution, due to the $1s2p\ ^1P_1 \rightarrow 1s2s\ ^1S_0$ transition, contributes only 0.0001 meV to the 70.4-meV width. The width of the $n = 2 \rightarrow n = 1$ transitions has been calculated using Drake's unified method [141], relativistic random phase approximation, MCDF, relativistic configuration interaction (RCI) and QED [142]. The effect of the negative energy continuum has been discussed in Refs. [135,143]. Radiative corrections to the photon emission have also been evaluated [144]. The differences between all theoretical values and our measurement are well within the experimental error bar.

B. Transition energies

We present in Fig. 5 the transition energy values obtained from the successive pairs of dispersive and nondispersive-

TABLE VII. Summary of all measured $n = 2 \rightarrow n = 1$ transition energies in He-like ions $7 \leq Z \leq 20$. The theoretical values are from Ref. [59], which are available for $Z \geq 12$. The experimental values are either reference-free measurements (RF) or measurements calibrated against standard reference x-ray transitions, or hydrogenlike transitions (SR).

Z	$1s2p\ ^1P_1 \rightarrow 1s^2\ ^1S_0$ (w)			$1s2p\ ^3P_2 \rightarrow 1s^2\ ^1S_0$ (x)			$1s2p\ ^3P_1 \rightarrow 1s^2\ ^1S_0$ (y)			$1s2s\ ^3S_1 \rightarrow 1s^2\ ^1S_0$ (z)			Method	Ref.
	Expt. (eV)	Err.	Theory	Expt. (eV)	Err.	Theory	Expt. (eV)	Err.	Theory	Expt. (eV)	Err.	Theory		
7	430.6870	0.0030											SR	[155]
8	573.949	0.011											SR	[155]
11	1126.72	0.31											SR	[33]
12	1352.329	0.015	1352.2483			1343.5417			1343.0988			1331.1118	SR	[33]
13	1598.46	0.31	1598.2914			1588.7611			1588.1254			1574.9799	SR	[33]
14	1864.76	0.42	1865.0014			1854.6679			1853.7804			1839.4495	SR	[33]
15	2152.84	0.56	2152.4310			2141.3188			2140.1082			2124.5619	SR	[33]
16	2461.27	0.49	2460.6292			2448.7628			2447.1439			2430.3512	SR	[33]
16	2460.69	0.15	2460.6292			2448.7628			2447.1439			2430.3512	SR	[36]
16	2460.630	0.021	2460.6292			2448.7628			2447.1439			2430.3512	RF	[7]
16	2460.670	0.090	2460.6292			2448.7628	2447.05	0.11	2447.1439			2430.3512	SR	[156]
18			3139.5821			3126.2896			3123.5344	3104.1605	0.0077	3104.1483	RF	[2]
18			3139.5821	3128	2	3126.2896			3123.5344			3104.1483	SR	[157]
18	3139.5927	0.0076	3139.5821			3126.2896			3123.5344			3104.1483	RF	This work
18	3139.5810	0.0092	3139.5821			3126.2896			3123.5344			3104.1483	RF	[7]
18	3139.552	0.037	3139.5821	3126.283	0.036	3126.2896	3123.521	0.036	3123.5344			3104.1483	SR	[40]
18	3139.57	0.25	3139.5821	3126.37	0.40	3126.2896	3123.57	0.24	3123.5344			3104.1483	SR	[35]
19	3510.58	0.12	3510.4616			3496.4937			3492.9736			3472.2417	SR	[158]
20	3902.43	0.18	3902.3777			3887.7607			3883.3169			3861.2059	SR	[36]
20	3902.19	0.12	3902.3777	3887.63	0.12	3887.7607	3883.24	0.12	3883.3169	3861.11	0.12	3861.2059	SR	[54]
21	4315.54	0.15	4315.4124			4300.1720			4294.6220			4271.0997	SR	[158]
21	4315.35	0.15	4315.4124	4300.23	0.15	4300.1720	4294.57	0.15	4294.6220	4271.19	0.15	4271.0997	SR	[53]
22	4749.73	0.17	4749.6441			4733.8008			4726.9373			4701.9746	SR	[158]
22	4749.852	0.072	4749.6441	4733.83	0.13	4733.8008	4727.07	0.10	4726.9373	4702.078	0.072	4701.9746	SR	[6]
23	5205.59	0.55	5205.1653			5188.7378			5180.3264			5153.8962	SR	[36]
23	5205.26	0.21	5205.1653			5188.7378			5180.3264			5153.8962	SR	[158]
23	5205.10	0.14	5205.1653	5189.120	0.210	5188.7378	5180.22	0.17	5180.3264	5153.82	0.14	5153.8962	SR	[159]

TABLE VIII. Summary of all measured $n = 2 \rightarrow n = 1$ transition energies in He-like ions $21 \leq Z \leq 92$. The theoretical values are from Ref. [59]. The experimental values are either reference-free measurements (RF) or measurements calibrated against standard reference x-ray transitions, or hydrogenlike transitions (SR).

Z	$1s2p\ ^1P_1 \rightarrow 1s^2\ ^1S_0$ (w)			$1s2p\ ^3P_2 \rightarrow 1s^2\ ^1S_0$ (x)			$1s2p\ ^3P_1 \rightarrow 1s^2\ ^1S_0$ (y)			$1s2s\ ^3S_1 \rightarrow 1s^2\ ^1S_0$ (z)			Method	Ref.
	Expt. (eV)	Err.	Theory	Expt. (eV)	Err.	Theory	Expt. (eV)	Err.	Theory	Expt. (eV)	Err.	Theory		
24	5682.66	0.52	5682.0684			5665.0715			5654.8491			5626.9276	SR	[36]
24	5682.32	0.40	5682.0684			5665.0715			5654.8491			5626.9276	SR	[158]
26	6700.76	0.36	6700.4347			6682.3339			6667.5786			6636.6126	SR	[36]
26	6700.73	0.20	6700.4347			6682.3339			6667.5786			6636.6126	SR	[158]
26	6700.441	0.049	6700.4347			6682.3339			6667.5786			6636.6126	RF	[7]
26	6700.90	0.25	6700.4347	6682.50	0.25	6682.3339	6667.50	0.25	6667.5786			6636.6126	SR	[160]
26	6700.549	0.070	6700.4347			6682.3339	6667.671	0.069	6667.5786			6636.6126	RF	[4]
27	7245.88	0.64	7242.1133			7223.4718			7205.9299			7173.4164	SR	[36]
28	7805.75	0.49	7805.6053			7786.4246			7765.7048			7731.6307	SR	[36]
29	8391.03	0.40	8391.0349			8371.3181			8346.9929			8311.3467	SR	[36]
29	8390.82	0.15	8391.0349	8371.17	0.15	8371.3181	8346.99	0.15	8346.9929	8310.83	0.15	8311.3467	SR	[8]
30	8997.53	0.65	8998.5238			8978.2677			8949.8740			8912.6466	SR	[36]
31	9627.45	0.75	9628.2072			9607.4099			9574.4461			9535.6292	SR	[36]
32	10 280.70	0.22	10 280.2175	10 259.52	0.37	10 258.8739	10 221.79	0.35	10 220.7996	10 181.33	0.52	10 180.3868	SR	[44]
36	13 115.45	0.30	13 114.4705			13 090.8657	13 026.8	3.0	13 026.1165			12 979.2656	SR	[161]
36	13 114.68	0.36	13 114.4705	13 091.17	0.37	13 090.8657	13 026.29	0.36	13 026.1165	12 979.63	0.41	12 979.2656	SR	[45]
36	13 114.47	0.14	13 114.4705			13 090.8657	13 026.15	0.14	13 026.1165			12 979.2656	RF	[9]
38	14 666.8	6.1	14 669.5399			14 644.7518			14 562.2995			14 512.1996	SR	[36]
39	15 475.6	2.9	15 482.1565			15 456.7619			15 364.1984			15 312.4664	SR	[36]
54	30 629.1	3.5	30 630.0512			30 594.3635	30 209.6	3.5	30 206.2652			30 129.1420	SR	[162]
54	30 619.9	4.0	30 630.0512			30 594.3635	30 210.5	4.5	30 206.2652	30 126.70	3.90	30 129.1420	SR	[163]
54	30 631.2	1.2	30 630.0512	30 594.50	1.70	30 594.3635	30 207.1	1.4	30 206.2652			30 129.1420	SR	[49]
59			37 003.7270			36 964.0900	36 389.1	6.8	36 391.2920			36 305.1570	SR	[47]
92	100 626	35	100 610.89			100 537.18			96 169.63			96 027.15	SR	[164]
92	100 598	107	100 610.89			100 537.18			96 169.63			96 027.15	SR	[165]

mode spectra, recorded during the experiment for the He-like argon $1s2p\ ^1P_1 \rightarrow 1s^2\ ^1S_0$ following the method presented in Sec. III. The weighted average and $\pm 1\sigma$ bands are plotted as well.

Table VI presents the measured He-like argon $1s2p\ ^1P_1 \rightarrow 1s^2\ ^1S_0$ transition energy, together with all known experimental and theoretical results. The final experimental accuracy, combining the instrumental contributions from Table I is

2.5×10^{-6} . The value is in agreement with a preliminary result, obtained with the same setup, but using fit with Voigt profiles of both the experimental spectra and the simulations [146,147]. The agreement with the most precise experiments, i.e., the two reference-free experiments [1,48] and the recoil ion experiment of Deslattes *et al.* [40] is well within combined error bars. The agreement with the calculation of Artemyev *et al.* [59] is also within the linearly combined error bars.

TABLE IX. Summary of all $n = 2 \rightarrow n = 1$ transition energies in He-like ions $Z \geq 7$, calibrated relative to the theoretical value of one of the four He-like transitions (x, y, z, or w). The line used as calibration is noted "Ref.". The energies of the measured lines have been re-evaluated using Ref. [59] for the reference transition energy. The displayed theoretical values are also from Ref. [59].

Z	$1s2p\ ^1P_1 \rightarrow 1s^2\ ^1S_0$ (w)			$1s2p\ ^3P_2 \rightarrow 1s^2\ ^1S_0$ (x)			$1s2p\ ^3P_1 \rightarrow 1s^2\ ^1S_0$ (y)			$1s2s\ ^3S_1 \rightarrow 1s^2\ ^1S_0$ (z)			Ref.
	Expt. (eV)	Err.	Theory	Expt. (eV)	Err.	Theory	Expt. (eV)	Err.	Theory	Expt. (eV)	Err.	Theory	
16			2460.6292	2448.739	0.020	2448.7628	2447.150	0.009	2447.1439	Ref.		2430.3512	[57]
18	3139.567	0.011	3139.5821	3126.291	0.011	3126.2896	3123.489	0.012	3123.5344	Ref.		3104.1483	[57]
18	Ref.		3139.5821	3126.440	0.079	3126.2896	3123.604	0.079	3123.5344	3104.21	0.16	3104.1483	[50]
21	Ref.		4315.4124	4300.00	0.30	4300.1720	4294.49	0.30	4294.6220	4271.99	0.29	4271.0997	[52]
22	Ref.		4749.6441	4733.86	0.18	4733.8008	4726.82	0.18	4726.9373	4701.89	0.18	4701.9746	[41]
23	Ref.		5205.1653	5188.18	0.43	5188.7378	5179.51	0.43	5180.3264	5153.24	0.43	5153.8962	[52]
24	Ref.		5682.0684	5664.67	0.52	5665.0715	5654.60	0.52	5654.8491	5626.63	0.51	5626.9276	[52]
25	Ref.		6180.4573	6163.25	0.61	6162.9043	6150.11	0.61	6150.5777	6120.66	0.60	6121.1432	[52]
28	Ref.		7805.6053	7786.96	0.49	7786.4246			7765.7048			7731.6307	[42]

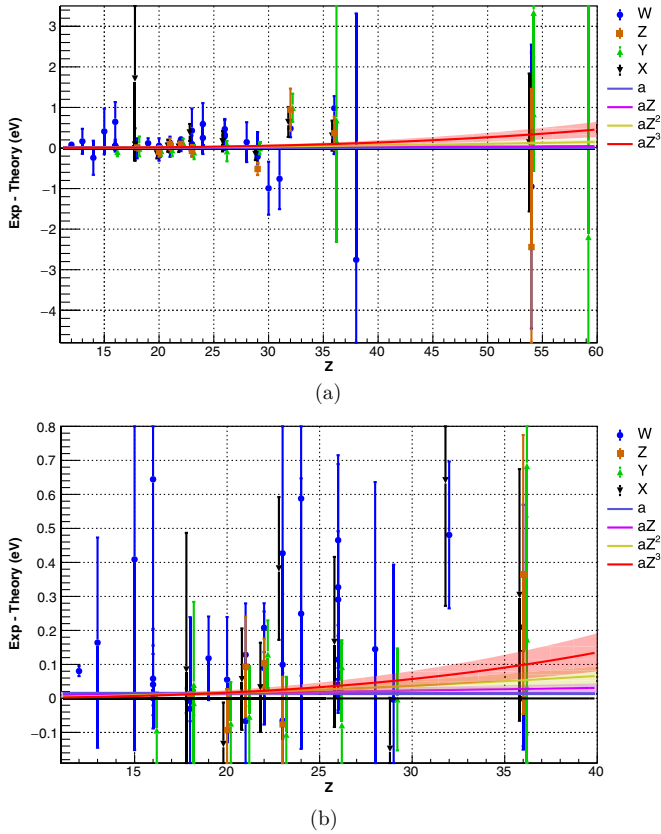


FIG. 6. Comparison between the theoretical values by Artemyev *et al.* [59] and experimental data for $n = 2 \rightarrow n = 1$ transition in He-like ions presented in Tables VII and VIII for all $12 \leq Z \leq 59$. (a) $12 \leq Z \leq 60$ range. (b) Zoom on the $12 \leq Z \leq 40$ range, and small energy differences. The continuous lines represent the weighted fits with a , aZ , aZ^2 , and aZ^3 functions, and the shaded area the $\pm 1\sigma$ bands, representing the 68% confidence interval from the fit. The experimental values for $Z = 92$ are not plotted as they have very large error bars, but were included in the fit. Values of different experiments for a given Z are slightly shifted horizontally to make the figure easier to read.

C. Comparison between measurements and calculations for $12 \leq Z \leq 92$

There have been many measurements of $n = 2 \rightarrow n = 1$ transition energies in He-like ions. The reference-free measurements, of the kind reported in the present work, and the measurements calibrated against x-ray standards or transitions in H-like ions are summarized in Tables VII and VIII for $7 \leq Z \leq 92$. Relative measurements, using the theoretical value for one of the He-like lines in the spectrum, originating from ECRIS or Tokamak experiments are summarized in Table IX. When older calculations were used as a reference, we used the energies of Ref. [59] to obtain an updated value for this table.

A detailed analysis of the difference between theory [59] and experiment has been performed in previous work [3,5,8]. Here we provide an updated analysis, which includes our new result and the data from Tables VII and VIII.

The differences between these experimental values and Artemyev *et al.* [59] theoretical values are plotted in Fig. 6 together with weighted fits by several functions of the shape

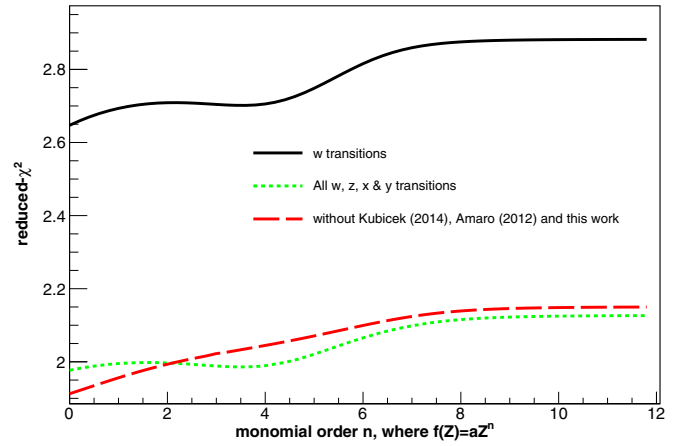


FIG. 7. Values of the reduced χ^2 function as a function of n , when fitting aZ^n , $n = 0$ to 12, to the experiment-theory differences from Tables VII and VIII. (Solid line) Reduced χ^2 fitting only the $1s2p^1P_1 \rightarrow 1s^2^1S_0$ (w) values. (Dotted line) Reduced χ^2 fitting all four w , x , y , and z transition energy differences with theory. (Dashed line) Same data as dotted line, but removing the reference-free values from this work and from Refs. [2,7].

aZ^n , $n = 0$ to 3. The $\pm 1\sigma$ error bands for the fits are also plotted. These error bands show that there is no significant deviation between theory and experiment.

In order to reinforce this conclusion, we have performed a systematic significance analysis. This analysis has been performed fitting functions of the form $f(Z) = aZ^n$, $n = 0, 12$ on three data sets built using the data presented in Tables VII and VIII. One data set contains only the w transition, one contains all w , x , y , and z transitions, and the last one is the same, from which the experimental values of this work of Kubicek *et al.* [7] and Amaro *et al.* [2] have been removed. The values of the reduced χ^2 are plotted as a function of n in Fig. 7 for the three subsets. It should be noted that the reduced χ^2 increases as a function of n , although in two of the subsets there is a weak local minimum near $n = 4$. We present in Fig. 8 the uncertainty of the fit coefficient a in standard-error units

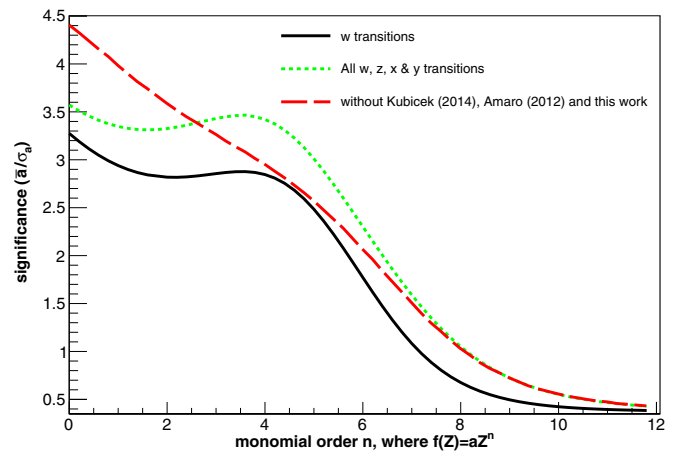


FIG. 8. Values of the significance of the fit coefficient in standard-error units as a function of n when fitting aZ^n to the experiment-theory differences from Tables VII and VIII.

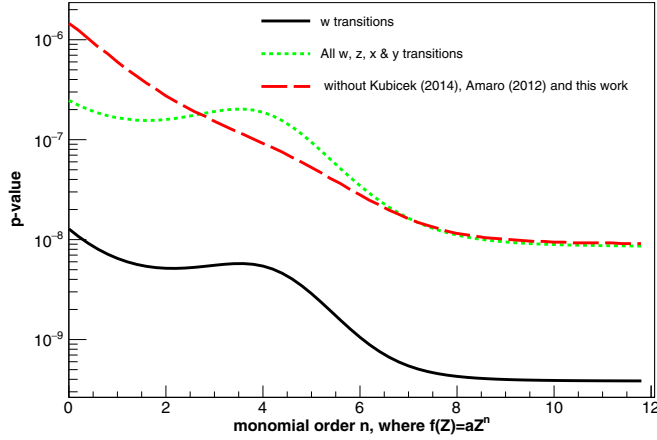


FIG. 9. p value as a function of n when fitting aZ^n to the experiment-theory differences from Tables VII and VIII. See legend of Fig. 8 for explanations of the data included in each curve.

as a function of n for all three data sets. The figure shows that the maximum deviation from zero is obtained for $n = 0$. The deviation of the fit coefficient tends to zero with increasing value of n while the reduced χ^2 increases. For the other two data sets considered, i.e., all experimental values presented in Tables VII and VIII or the subset consisting only of the w lines, there is a local maximum for each data set around $n = 4$. For all experimental data the local maximum happens at $n \simeq 4.2$ with a coefficient significance of 3.5 standard errors, while for the w lines the local maximum is at $n \simeq 3.8$ with a deviation of 3 standard errors from zero. In spite of the presence of this local maximum for different monomial orders of n , the maximum deviation from zero of the fit parameter is at $n = 0$ as well as the minimum reduced χ^2 value. This leads to the conclusion that $f(Z) = aZ^0$ is the most probable model to describe the data when considering a power law dependence with Z .

To sustain this conclusion, a χ^2 goodness of a fit test was performed. Figure 9 shows the result probability (p value) of the observed χ^2 cumulative distribution function (upper tail) as a function of n , for the given number of degrees of freedom and the minimum χ^2 value of each performed fit. This probability, that the observed χ^2_{obs} for ν degrees of freedom is larger than χ^2 , is given by [90]

$$p(\chi^2, \nu) = Q\left(\frac{\chi^2}{2}, \frac{\nu}{2}\right), \quad (7)$$

where Q is the incomplete Γ function. When all data from Tables VII and VIII are included, $\nu = 85 - 1$. It can be noticed

TABLE X. Measured and computed natural line width values for the $1s2s^22p^1P_1 \rightarrow 1s^22s^2^1S_0$ transition in Be-like Ar. All values are given in meV, and estimated uncertainties are shown in parentheses.

Transition	Experiment	Theory	Reference
$1s2s^22p^1P_1 \rightarrow 1s^22s^2^1S_0$	146 (18)	128 (40)	MCDF (this work)
		121.4	FAC (this work)
		150.9	Costa <i>et al.</i> (2001) [139]
		146.8	Chen (1985) [99]
		106.1	Safronova <i>et al.</i> (1979) [98]

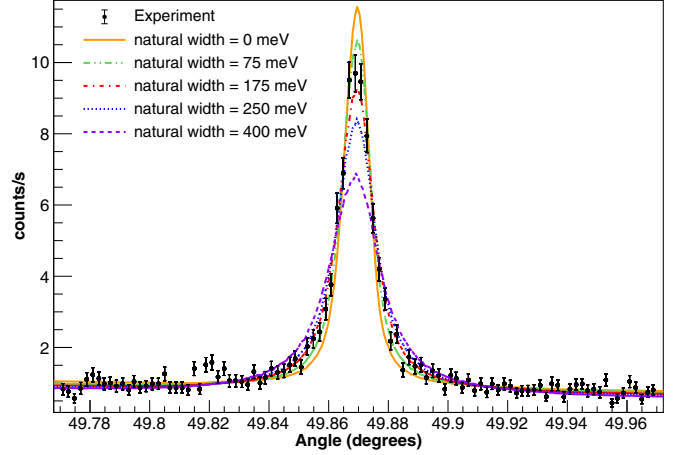


FIG. 10. Example of a dispersive-mode experimental spectrum for the Be-like Ar $1s2s^22p^1P_1 \rightarrow 1s^22s^2^1S_0$ transition (black dots), together with a few plots of the function in Eq. (1), for different values of the natural line width Γ_L^i . The four parameters have been adjusted to minimize the reduced $\chi^2(\Gamma_L)$ (see text for more explanations).

that the highest p value for the three considered data sets is for $n = 0$, and, as before, one can see a local maximum when considering all experimental results from Tables VII and VIII or just the w lines for the same n value as from Fig. 8. Considering the standard significance level of 0.05 to evaluate the acceptance or rejection of the null hypotheses (i.e., the fact that the data can be described by the aZ^n function), and since the highest p value is 1.4×10^{-6} for the three considered data sets, the null hypotheses has a very small probability to be true, with the caveats noted in Ref. [154]. We also performed a t -student test, which shows that $a = 0$ is the most probable value for all n . Therefore, we conclude that it is highly unlikely that the experiment-theory difference has a dependence in Z of the form $f(Z) = aZ^n$ for any given n with $0 \leq n \leq 12$.

VI. RESULTS AND COMPARISON WITH THEORY FOR THE BE-LIKE $1s2s^22p^1P_1 \rightarrow 1s^22s^2^1S_0$ TRANSITION

A typical spectrum for the $1s2s^22p^1P_1 \rightarrow 1s^22s^2^1S_0$ transition, obtained in dispersive mode, is presented in Fig. 10. The width of the $1s2s^22p^1P_1$ in contrast to the He-like case, has both radiative and nonradiative (Auger) contributions. The radiative part is also heavily dominated by the $1s2s^22p^1P_1 \rightarrow 1s^22s^2^1S_0$ transition. As seen in Table IV, the nonradiative part is mostly due to three Auger transitions: $1s2s^22p^1P_1 \rightarrow 1s^22s^2^2S_{1/2}$, $1s2s^22p^1P_1 \rightarrow 1s^22p^2P_{1/2}$, and $1s2s^22p^1P_1 \rightarrow 1s^22p^2P_{3/2}$. The radiative and nonradiative contributions are

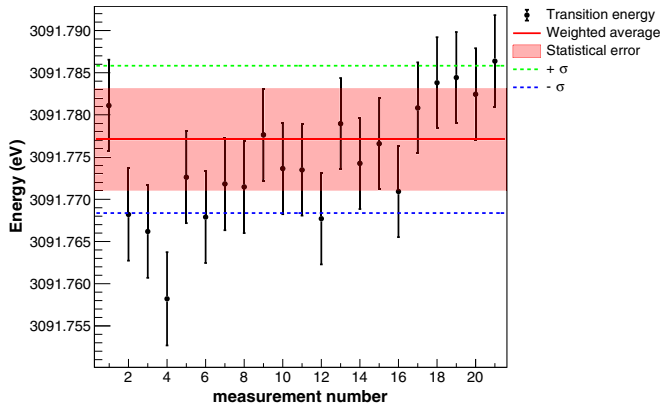


FIG. 11. Be-like argon $1s2s^22p^1P_1 \rightarrow 1s^22s^2^1S_0$ transition energy values for the different spectra recorded during the experiment. Error bars in each point correspond to the quadratic sum of the peak fitting uncertainty with the uncertainties from Table I, which have random fluctuations only, i.e., the angle measurement and the temperature correction. The (pink) shaded area corresponds to the weighted average of the peak position statistical uncertainty obtained from the fit. The $\pm 1\sigma$ lines combine these statistical uncertainties with all systematic errors from Table I. Every pair of points corresponds to one-day data taking (see text for explanations).

of similar size. The distribution of results from the daily experiments is presented in Fig. 3(b). Our experimental width and the comparison with theory are presented in Table X. The agreement between theory and experiment is within combined experimental and theoretical uncertainty.

We present in Fig. 11 the transition energy values obtained from the successive pairs of dispersive and nondispersive-mode spectra, recorded during the experiment for the $1s2s^22p^1P_1 \rightarrow 1s^22s^2^1S_0$ transition, following the method presented in Sec. III. The weighted average and $\pm 1\sigma$ values are plotted as well.

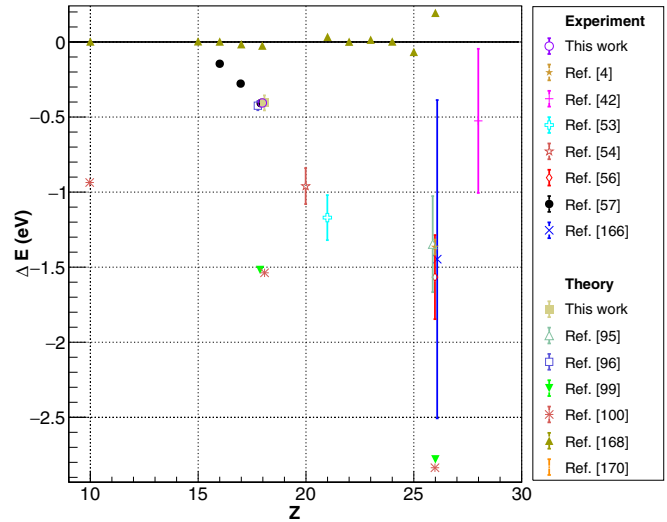


FIG. 12. Comparison between experimental and theoretical values for the $1s2s^22p^1P_1 \rightarrow 1s^22s^2^1S_0$ transition energies, as a function of Z . All values are compared to the energies in Ref. [98]. The experimental results are from the following references: Schlessler *et al.* (2013) [57], Beiersdorfer *et al.* (1993) [56], Decaux *et al.* (1997) [166], Rudolph *et al.* (2013) [4], Hsuan *et al.* (1987) [42], Rice *et al.* (1995) [53], Rice *et al.* (2014) [54]. The theoretical results are from the following references: Yerokhin *et al.* (2015) [96], Yerokhin *et al.* (2014) [95], Chen and Crasemann (1987) [100], Chen (1985) [99], Shuqiang *et al.* (2006) [170], Safronova and Shlyaptseva (1996) [168].

In Table XI, we present our results for the $1s2s^22p^1P_1 \rightarrow 1s^22s^2^1S_0$ transition energies. The measurement has been performed with a relative uncertainty of 2.8×10^{-6} . The difference with the Yerokhin *et al.* calculation [96], which is given with a relative accuracy of 11×10^{-6} , is 9.7×10^{-6} . The difference with our MCDF results using effective operator self-energy screening is 2.3×10^{-6} , while it is 3.6×10^{-6}

TABLE XI. Comparison between experimental and theoretical Be-like argon $1s2s^22p^1P_1 \rightarrow 1s^22s^2^1S_0$ transition energies. All energies are given in eV, and estimated uncertainties are shown in parentheses.

Transition energy	Reference
	Experiment
3091.7771(61)(63)(87)	This work(stat.)(syst.)(tot.)
3091.776(3)	Schlessler <i>et al.</i> (2013) [57]
	Theory
3091.716(30)(18)(11)	This work using model operators [77,127] (see Table II) (Corr.)(SE screening)(Auger shift)
3091.710 (30)(16)(11)	This work using Welton model(see Table II)(Corr.)(SE screening)(Auger shift)
3091.11	This work using FAC [138]
3091.749 (34)	Yerokhin <i>et al.</i> (2015) [96]
3088.958	Natarajan (2003) [140]
3091.95	Costa <i>et al.</i> (2001) [139]
3092.157	Safronova and Shlyaptseva (1996) [168]
3090.64	Chen and Crasemann (1987) [100]
3090.66	Chen (1985) [99]
3092.18	Safronova and Lisina (1979) [98]
3092.18	Boiko <i>et al.</i> (1978) [169]

TABLE XII. Comparison between relative measurements from Ref. [57], and the values deduced from this work and our previous measurement of the $1s2s^3S_1 \rightarrow 1s^2^1S_0$ M1 transition [2] for the $1s2p^1P_1 \rightarrow 1s^2^1S_0$ and the $1s2s^2p^1P_1 \rightarrow 1s^2s^2^1S_0$ transitions. All energies are given in eV, and uncertainties are shown in parentheses.

Level	Experiment		Theory	
	This work, Ref. [2]	Ref. [57]	Refs. [59,96]	This work
$1s2p^1P_1$	35.432(10)	35.419(11)	35.4337(4)	35.434
$1s2s^2p^1P_1$	-12.383(11)	-12.372(3)	-12.399(34)	-12.403

with the calculation using the Welton method. The difference between the present reference-free measurement and the relative measurement presented in Ref. [57], calibrated against the theoretical value of the $1s2s^3S_1 \rightarrow 1s^2^1S_0$ transition energy of [59] is only 0.4×10^{-6} . All recent measurements and calculations are thus forming a very coherent set of data.

The energy of this transition has not been extensively studied. It was measured relative either to theoretical values in S, Cl, and Ar [57], Sc [53], Fe [56,166], Ni [42], and Pr [47] or to K edges in Fe [4]. The width and Auger rate for this transition have also been measured in iron [4,167], with the combined use of synchrotron radiation and ion production with an EBIT. In Fig. 12, we present a comparison between theory and experiment, and between different calculations for the $1s2s^2p^1P_1 \rightarrow 1s^2s^2^1S_0$ line energy, for $10 \leq Z \leq 29$. Since there is no recent calculation covering all elements for which there is a measured value, we use as reference the old calculation from Ref. [98], which does not include accurate QED corrections.

To conclude the discussion on both transitions measured here, we have subtracted the $1s2s^3S_1 \rightarrow 1s^2^1S_0$ M1 transition energy measured with the same method in Ref. [2] from the energies of the $1s2p^1P_1 \rightarrow 1s^2^1S_0$ and the $1s2s^2p^1P_1 \rightarrow 1s^2s^2^1S_0$ transition energies measured here (Table XII). The agreement with the relative measurements performed in Ref. [57] is within combined error bars. The difference between the reference-free transition measurements are in even better agreement with theory than the direct measurements reported in Ref. [57].

VII. CONCLUSIONS

In the present work, we report the reference-free measurement of two x-ray transition energies and widths in He-like ($1s2p^1P_1 \rightarrow 1s^2^1S_0$) and Be-like ($1s2s^2p^1P_1 \rightarrow 1s^2s^2^1S_0$) argon ions. The measurement of the $1s2s^2p^1P_1 \rightarrow 1s^2s^2^1S_0$ transition energy is the first reference-free measurement for a transition of an ion with more than two electrons. The measurements were made with a double-crystal spectrometer connected to an ECRIS. The data analysis was performed using a dedicated x-ray tracing simulation code that includes the physical characteristics and geometry of the detector. The energy measurements agree within the error bars with the most accurate calculations and with other recent measurements. The measurement of the He-like transition is one of the five measurements with a relative accuracy below 1×10^{-5} . The measurement of the Be-like Ar transition is the first reference-free measurement

on such a transition, and the only one with this level accuracy, except for measurements relative to nearby He-like transitions.

We have also performed MCDF calculations of the transition energies and widths, using both the MCDFGME code, with improved self-energy screening and the RCI flexible atomic code FAC and compared with all existing theoretical and experimental results available to us. The MCDFGME theoretical results are in agreement with existing experimental results and with the most advanced calculations available.

We have analyzed the difference between all available $n = 2 \rightarrow n = 1$ experimental transition energies in He-like ions for $Z \geq 12$ and the theoretical results from Ref. [59]. When taking into account the recent high-precision, reference-free measurements in heliumlike argon [1,2,7] and the present result, in He-like iron[4], and in He-like krypton[9] from the Heidelberg and Paris groups, as well as the copper result [8] by the Livermore group, we have shown that there is no significant Z -dependent deviation between the most advanced theory and experiment.

The method presented here will be extended to other charge states like lithiumlike or boronlike ions, and nearby elements in the near future.

ACKNOWLEDGMENTS

This research was supported in part by Projects No. PEStOE/FIS/UI0303/2011 and No. PTDC/FIS/117606/2010, and by research center Grant No. UID/FIS/04559/2013 (LIB-Phys), from FCT/MCTES/PIDDAC, Portugal. We acknowledge partial support from NIST (P.I.), from PESSOA Huber Curien Program No. 38028UD, and PAULF Program No. 2017-C08. P.A., J.M., and M.G. acknowledge support from FCT under Contracts No. SFRH/BPD/92329/2013, No. SFRH/BD/52332/2013, and No. SFRH/BPD/92455/2013, respectively. Laboratoire Kastler Brossel (LKB) is “Unité Mixte de Recherche de Sorbonne Université, de ENS-PSL Research University, du Collège de France et du CNRS No. 8552.” P.I. is a member of the Allianz Program of the Helmholtz Association, Contract No. EMMI HA-216 “Extremes of Density and Temperature: Cosmic Matter in the Laboratory.” The SIMPA ECRIS has been financed by grants from CNRS, MESR, and University Pierre and Marie Curie (now Sorbonne Université). The experiment has been supported by BNM Grant No. 0130002 and ANR Grant No. ANR-06-BLAN-0223. We wish to thank Jean-Paul Desclaux for his help improving the MCDFGME code, and Dr. Martino Trassinelli (INSP) for valuable discussions and his help during early stages of the experiment.

- [1] H. Bruhns, J. Braun, K. Kubiček, J. R. Crespo López-Urrutia, and J. Ullrich, *Phys. Rev. Lett.* **99**, 113001 (2007).
- [2] P. Amaro, S. Schlessler, M. Guerra, E. O. Le Bigot, J.-M. Isac, P. Travers, J. P. Santos, C. I. Szabo, A. Gumberidze, and P. Indelicato, *Phys. Rev. Lett.* **109**, 043005 (2012).
- [3] C. T. Chantler, M. N. Kinnane, J. D. Gillaspay, L. T. Hudson, A. T. Payne, L. F. Smale, A. Henins, J. M. Pomeroy, J. N. Tan, J. A. Kimpton *et al.*, *Phys. Rev. Lett.* **109**, 153001 (2012).
- [4] J. K. Rudolph, S. Bernitt, S. W. Epp, R. Steinbrügge, C. Beilmann, G. V. Brown, S. Eberle, A. Graf, Z. Harman, N. Hell *et al.*, *Phys. Rev. Lett.* **111**, 103002 (2013).
- [5] C. T. Chantler, A. T. Payne, J. D. Gillaspay, L. T. Hudson, L. F. Smale, A. Henins, J. A. Kimpton, and E. Takács, *New J. Phys.* **16**, 123037 (2014).
- [6] A. T. Payne, C. T. Chantler, M. N. Kinnane, J. D. Gillaspay, L. T. Hudson, L. F. Smale, A. Henins, J. A. Kimpton, and E. Takacs, *J. Phys. B: At. Mol. Opt. Phys.* **47**, 185001 (2014).
- [7] K. Kubiček, P. H. Mokler, V. Mäckel, J. Ullrich, and J. R. Crespo López-Urrutia, *Phys. Rev. A* **90**, 032508 (2014).
- [8] P. Beiersdorfer and G. V. Brown, *Phys. Rev. A* **91**, 032514 (2015).
- [9] S. W. Epp, R. Steinbrügge, S. Bernitt, J. K. Rudolph, C. Beilmann, H. Bekker, A. Müller, O. O. Versolato, H. C. Wille, H. Yavaş *et al.*, *Phys. Rev. A* **92**, 020502 (2015).
- [10] S. Sturm, A. Wagner, B. Schabinger, J. Zatorski, Z. Harman, W. Quint, G. Werth, C. H. Keitel, and K. Blaum, *Phys. Rev. Lett.* **107**, 023002 (2011).
- [11] A. Wagner, S. Sturm, F. Köhler, D. A. Glazov, A. V. Volotka, G. Plunien, W. Quint, G. Werth, V. M. Shabaev, and K. Blaum, *Phys. Rev. Lett.* **110**, 033003 (2013).
- [12] S. Sturm, F. Köhler, J. Zatorski, A. Wagner, Z. Harman, G. Werth, W. Quint, C. H. Keitel, and K. Blaum, *Nature (London)* **506**, 467 (2014).
- [13] F. Köhler, S. Sturm, A. Kracke, G. Werth, W. Quint, and K. Blaum, *J. Phys. B: At. Mol. Opt. Phys.* **48**, 144032 (2015).
- [14] J. Ullmann, Z. Andelkovic, A. Dax, W. Geithner, C. Geppert, C. Gorges, M. Hammen, V. Hannen, S. Kaufmann, K. König *et al.*, *J. Phys. B: At. Mol. Opt. Phys.* **48**, 144022 (2015).
- [15] J. P. Marques, P. Indelicato, F. Parente, J. M. Sampaio, and J. P. Santos, *Phys. Rev. A* **94**, 042504 (2016).
- [16] V. A. Yerokhin, E. Berseneva, Z. Harman, I. I. Tupitsyn, and C. H. Keitel, *Phys. Rev. A* **94**, 022502 (2016).
- [17] P. Beiersdorfer, A. L. Osterheld, J. H. Scofield, J. R. Crespo López-Urrutia, and K. Widmann, *Phys. Rev. Lett.* **80**, 3022 (1998).
- [18] P. Seelig, S. Borneis, A. Dax, T. Engel, S. Faber, M. Gerlach, C. Holbrow, G. Huber, T. Kühl, D. Marx *et al.*, *Phys. Rev. Lett.* **81**, 4824 (1998).
- [19] S. Boucard and P. Indelicato, *Eur. Phys. J. D* **8**, 59 (2000).
- [20] P. Beiersdorfer, S. B. Utter, K. L. Wong, J. R. Crespo López-Urrutia, J. A. Britten, H. Chen, C. L. Harris, R. S. Thoe, D. B. Thorn, E. Träbert *et al.*, *Phys. Rev. A* **64**, 032506 (2001).
- [21] V. A. Yerokhin and V. M. Shabaev, *Phys. Rev. A* **64**, 012506 (2001).
- [22] V. M. Shabaev, A. N. Artemyev, V. A. Yerokhin, O. M. Zherebtsov, and G. Soff, *Phys. Rev. Lett.* **86**, 3959 (2001).
- [23] A. V. Volotka, D. A. Glazov, O. V. Andreev, V. M. Shabaev, I. I. Tupitsyn, and G. Plunien, *Phys. Rev. Lett.* **108**, 073001 (2012).
- [24] O. V. Andreev, D. A. Glazov, A. V. Volotka, V. M. Shabaev, and G. Plunien, *Phys. Rev. A* **85**, 022510 (2012).
- [25] W. Nörtershäuser, M. Lochmann, R. Jöhren, C. Geppert, Z. Andelkovic, D. Anielski, B. Botermann, M. Bussmann, A. Dax, N. Frömmgen *et al.*, *Phys. Scr.* **T156**, 014016 (2013).
- [26] M. Lochmann, R. Jöhren, C. Geppert, Z. Andelkovic, D. Anielski, B. Botermann, M. Bussmann, A. Dax, N. Frömmgen, M. Hammen *et al.*, *Phys. Rev. A* **90**, 030501 (2014).
- [27] P. Beiersdorfer, E. Träbert, G. V. Brown, J. Clementson, D. B. Thorn, M. H. Chen, K. T. Cheng, and J. Sapirstein, *Phys. Rev. Lett.* **112**, 233003 (2014).
- [28] J. Vollbrecht, Z. Andelkovic, A. Dax, W. Geithner, C. Geppert, C. Gorges, M. Hammen, V. Hannen, S. Kaufmann, K. König *et al.*, *J. Phys.: Conf. Ser.* **583**, 012002 (2015).
- [29] J. Ullmann, Z. Andelkovic, C. Brandau, A. Dax, W. Geithner, C. Geppert, C. Gorges, M. Hammen, V. Hannen, S. Kaufmann *et al.*, *Nat. Commun.* **8**, 15484 (2017).
- [30] R. Pohl, A. Antognini, F. Nez, F. D. Amaro, F. Biraben, J. M. R. Cardoso, D. S. Covita, A. Dax, S. Dhawan, L. M. P. Fernandes *et al.*, *Nature (London)* **466**, 213 (2010).
- [31] A. Antognini, F. Nez, K. Schuhmann, F. D. Amaro, F. Biraben, J. M. R. Cardoso, D. S. Covita, A. Dax, S. Dhawan, M. Diepold *et al.*, *Science* **339**, 417 (2013).
- [32] R. Pohl, F. Nez, L. M. P. Fernandes, F. D. Amaro, F. Biraben, J. M. R. Cardoso, D. S. Covita, A. Dax, S. Dhawan, M. Diepold *et al.*, *Science* **353**, 669 (2016).
- [33] E. V. Aglitskii, V. A. Boiko, S. M. Zakharov, S. A. Pikuz, and A. Y. Faenov, *Sov. J. Quantum Electron.* **4**, 500 (1974).
- [34] H. D. Dohmann and R. Mann, *Z. Phys. A* **291**, 15 (1979).
- [35] J. P. Briand, J. P. Mosse, P. Indelicato, P. Chevallier, D. Girard-Vernhet, A. Chetoui, M. T. Ramos, and J. P. Desclaux, *Phys. Rev. A* **28**, 1413 (1983).
- [36] E. V. Aglitsky, P. S. Antsiferov, S. L. Mandelstam, A. M. Panin, U. I. Safronova, S. A. Ulitin, and L. A. Vainshtein, *Phys. Scr.* **38**(2), 136 (1988).
- [37] T. Stöhlker, P. H. Mokler, K. Beckert, F. Bosch, H. Eickhoff, B. Franzke, H. Geissel, M. Jung, T. Kandler, O. Klepper *et al.*, *Nucl. Instrum. Methods Phys. Res., Sect. B* **87**, 64 (1994).
- [38] T. Stöhlker, P. H. Mokler, F. Bosch, R. W. Dunford, F. Franzke, O. Klepper, C. Kozhuharov, T. Ludziejewski, F. Nolden, H. Reich *et al.*, *Phys. Rev. Lett.* **85**, 3109 (2000).
- [39] A. Gumberidze, T. Stöhlker, D. Banaś, K. Beckert, P. Beller, H. F. Beyer, F. Bosch, S. Hagmann, C. Kozhuharov, D. Liesen *et al.*, *Phys. Rev. Lett.* **94**, 223001 (2005).
- [40] R. D. Deslattes, H. F. Beyer, and F. Folkmann, *J. Phys. B: At. Mol. Phys.* **17**, L689 (1984).
- [41] M. Bitter, K. W. Hill, M. Zarnstorff, S. von Goeler, R. Hulse, L. C. Johnson, N. R. Sauthoff, S. Sesnic, K. M. Young, M. Tavernier *et al.*, *Phys. Rev. A* **32**, 3011 (1985).
- [42] H. Hsuan, M. Bitter, K. W. Hills, S. von Goeler, B. Grek, D. Johnson, L. C. Johnson, S. Sesnic, C. P. Bhalla, K. R. Karim *et al.*, *Phys. Rev. A* **35**, 4280 (1987).
- [43] W. M. Neupert, *Sol. Phys.* **18**, 474 (1971).
- [44] S. MacLaren, P. Beiersdorfer, D. A. Vogel, D. Knapp, R. E. Marrs, K. Wong, and R. Zasadzinski, *Phys. Rev. A* **45**, 329 (1992).
- [45] K. Widmann, P. Beiersdorfer, V. Decaux, and M. Bitter, *Phys. Rev. A* **53**, 2200 (1996).
- [46] P. Beiersdorfer, J. A. Britten, G. V. Brown, H. Chen, E. J. Clothiaux, J. Cottam, E. Forster, M. F. Gu, C. L. Harris, S. M. Kahn *et al.*, *Phys. Scr.* **T92**, 268 (2001).

- [47] D. B. Thorn, G. V. Brown, J. H. T. Clementson, H. Chen, M. Chen, P. Beiersdorfer, K. R. Boyce, C. A. Kilbourne, F. S. Porter, and R. L. Kelley, *Can. J. Phys.* **86**, 241 (2008).
- [48] K. Kubiček, J. Braun, H. Bruhns, J. R. Crespo López-Urrutia, P. H. Mokler, and J. Ullrich, *Rev. Sci. Instrum.* **83**, 013102 (2012).
- [49] D. B. Thorn, M. F. Gu, G. V. Brown, P. Beiersdorfer, F. S. Porter, C. A. Kilbourne, and R. L. Kelley, *Phys. Rev. Lett.* **103**, 163001 (2009).
- [50] TFR Group, F. Bombarda, F. Bely-Dubau, P. Faucher, M. Cornille, J. Dubau, and M. Loulergue, *Phys. Rev. A* **32**, 2374 (1985).
- [51] J. E. Rice, M. L. Reinke, J. M. A. Ashbourn, C. Gao, M. Bitter, L. Delgado-Aparicio, K. Hill, N. T. Howard, J. W. Hughes, and U. I. Safronova, *J. Phys. B: At. Mol. Opt. Phys.* **48**, 144013 (2015).
- [52] TFR Group, M. Cornille, J. Dubau, and M. Loulergue, *Phys. Rev. A* **32**, 3000 (1985).
- [53] J. E. Rice, M. A. Graf, J. L. Terry, E. S. Marmar, K. Giesing, and F. Bombarda, *J. Phys. B: At. Mol. Opt. Phys.* **28**, 893 (1995).
- [54] J. E. Rice, M. L. Reinke, J. M. A. Ashbourn, C. Gao, M. M. Victora, M. A. Chilenski, L. Delgado-Aparicio, N. T. Howard, A. E. Hubbard, J. W. Hughes *et al.*, *J. Phys. B: At. Mol. Opt. Phys.* **47**, 075701 (2014).
- [55] P. Beiersdorfer, M. H. Chen, R. E. Marrs, M. B. Schneider, and R. S. Walling, *Phys. Rev. A* **44**, 396 (1991).
- [56] P. Beiersdorfer, T. Phillips, V. L. Jacobs, K. W. Hill, M. Bitter, S. von Goeler, and S. M. Kahn, *Astrophys. J.* **409**, 846 (1993).
- [57] S. Schlessler, S. Boucard, D. S. Covita, J. M. F. dos Santos, H. Fuhrmann, D. Gotta, A. Gruber, M. Hennebach, A. Hirtl, P. Indelicato *et al.*, *Phys. Rev. A* **88**, 022503 (2013).
- [58] C. T. Chantler and J. A. Kimpton, *Can. J. Phys.* **87**, 763 (2009).
- [59] A. N. Artemyev, V. M. Shabaev, V. A. Yerokhin, G. Plunien, and G. Soff, *Phys. Rev. A* **71**, 062104 (2005).
- [60] G. Plunien, B. Müller, W. Greiner, and G. Soff, *Phys. Rev. A* **43**, 5853 (1991).
- [61] G. Plunien and G. Soff, *Phys. Rev. A* **51**, 1119 (1995).
- [62] G. Plunien and G. Soff, *Phys. Rev. A* **53**, 4614 (1996).
- [63] T. Beier, P. J. Mohr, H. Persson, and G. Soff, *Phys. Rev. A* **58**, 954 (1998).
- [64] K. S. E. Eikema, W. Ubachs, W. Vassen, and W. Hogervorst, *Phys. Rev. Lett.* **76**, 1216 (1996).
- [65] K. S. E. Eikema, W. Ubachs, W. Vassen, and W. Hogervorst, *Phys. Rev. A* **55**, 1866 (1997).
- [66] D. Z. Kandula, C. Gohle, T. J. Pinkert, W. Ubachs, and K. S. E. Eikema, *Phys. Rev. A* **84**, 062512 (2011).
- [67] K. Pachucki, *J. Phys. B: At. Mol. Opt. Phys.* **31**, 2489 (1998).
- [68] K. Pachucki, *J. Phys. B: At. Mol. Opt. Phys.* **31**, 3547 (1998).
- [69] K. Pachucki, *Phys. Rev. A* **74**, 022512 (2006).
- [70] K. Pachucki, *Phys. Rev. A* **74**, 062510 (2006).
- [71] V. A. Yerokhin and K. Pachucki, *Phys. Rev. A* **81**, 022507 (2010).
- [72] I. Angeli and K. P. Marinova, *At. Data Nucl. Data Tables* **99**, 69 (2013).
- [73] E. Bulbul, M. Markevitch, A. Foster, R. K. Smith, M. Loewenstein, and W. R. Scott, *Astrophys. J.* **789**, 13 (2014).
- [74] A. Boyarsky, O. Ruchayskiy, D. Iakubovskiy, and J. Franse, *Phys. Rev. Lett.* **113**, 251301 (2014).
- [75] C. Shah, S. Dobrodey, S. Bernitt, R. Steinbrügge, J. R. Crespo López-Urrutia, L. Gu, and J. Kaastra, *Astrophys. J.* **833**, 52 (2016).
- [76] F. A. Aharonian, H. Akamatsu, F. Akimoto, S. W. Allen, L. Angelini, K. A. Arnaud, M. Audard, H. Awaki, M. Axelsson, A. Bamba *et al.*, *Astrophys. J. Lett.* **837**, L15 (2017).
- [77] V. M. Shabaev, I. I. Tupitsyn, and V. A. Yerokhin, *Phys. Rev. A* **88**, 012513 (2013).
- [78] R. D. Deslattes, *Rev. Sci. Instrum.* **38**, 815 (1967).
- [79] P. Amaro, C. I. Szabo, S. Schlessler, A. Gumberidze, E. G. Kessler Jr., A. Henins, E. O. Le Bigot, M. Trassinelli, J. M. Isac, P. Travers *et al.*, *Radiat. Phys. Chem.* **98**, 132 (2014).
- [80] E. G. Kessler Jr., R. D. Deslattes, and A. Henins, *Phys. Rev. A* **19**, 215 (1979).
- [81] A. Gumberidze, M. Trassinelli, N. Adrouche, C. I. Szabo, P. Indelicato, F. Haranger, J. M. Isac, E. Lamour, E. O. Le Bigot, J. Merot *et al.*, *Rev. Sci. Instrum.* **81**, 033303 (2010).
- [82] M. Guerra, P. Amaro, C. I. Szabo, A. Gumberidze, P. Indelicato, and J. P. Santos, *J. Phys. B: At. Mol. Opt. Phys.* **46**, 065701 (2013).
- [83] H. Fujimoto, A. Waseda, and X. W. Zhang, *Metrologia* **48**, S55 (2011).
- [84] P. Mohr, B. Taylor, and D. Newell, *Rev. Mod. Phys.* **84**, 1527 (2012).
- [85] E. G. Kessler Jr., C. I. Szabo, J. P. Cline, A. Henins, L. T. Hudson, M. H. Mendenhall, and M. D. Vaudin, *J. Res. Natl. Inst. Stand. Technol.* **122**, 24 (2017).
- [86] M. Sanchez del Rio and R. J. Dejus, *Proc. SPIE* **5536**, 171 (2004).
- [87] W. H. Zachariasen, *Theory of X-ray Diffraction in Crystals* (Dover Publications, New York, 1967).
- [88] S. Stepanov, <http://sergey.gmca.aps.anl.gov/x0h.html>.
- [89] O. M. Lugovskaya and S. A. Stepanov, *Sov. Phys. Crystallogr.* **36**, 478 (1991).
- [90] W. H. Press, B. P. Flannery, S. A. Teukolsky, and W. T. Vetterling, *Numerical Recipes 3rd Edition: The Art of Scientific Computing* (Cambridge University Press, Cambridge, 2007).
- [91] R. Brun and F. Rademakers, *Nucl. Instrum. Methods A* **389**, 81 (1997).
- [92] I. Antcheva, M. Ballintijn, B. Bellenot, M. Biskup, R. Brun, N. Buncic, P. Canal, D. Casadei, O. Couet, V. Fine *et al.*, *Comput. Phys. Commun.* **180**, 2499 (2009).
- [93] I. Antcheva, M. Ballintijn, B. Bellenot, M. Biskup, R. Brun, N. Buncic, P. Canal, D. Casadei, O. Couet, V. Fine *et al.*, *Comput. Phys. Commun.* **182**, 1384 (2011).
- [94] Wolfram Research, Computer code MATHEMATICA 11.0, Wolfram, Champaign, 2016.
- [95] V. A. Yerokhin, A. Surzhykov, and S. Fritzsche, *Phys. Rev. A* **90**, 022509 (2014).
- [96] V. A. Yerokhin, A. Surzhykov, and S. Fritzsche, *Phys. Scr.* **90**, 054003 (2015).
- [97] U. I. Safronova and A. M. Urnov, *J. Phys. B: At. Mol. Opt. Phys.* **12**, 3171 (1979).
- [98] U. I. Safronova and T. G. Lisina, *At. Data Nucl. Data Tables* **24**, 49 (1979).
- [99] M. H. Chen, *Phys. Rev. A* **31**, 1449 (1985).
- [100] M. H. Chen and B. Crasemann, *At. Data Nucl. Data Tables* **37**, 419 (1987).

- [101] J. P. Desclaux, *Comput. Phys. Commun.* **9**, 31 (1975).
- [102] P. Indelicato and J. P. Desclaux, *Phys. Rev. A* **42**, 5139 (1990).
- [103] P. Indelicato, O. Gorcex, and J. P. Desclaux, *J. Phys. B: At. Mol. Opt. Phys.* **20**, 651 (1987).
- [104] P. Indelicato and J. Desclaux, MCDFGME: A Multiconfiguration Dirac Fock and General Matrix Elements Program (release 2005), 2005, <http://kroll.lkb.upmc.fr/mcdf>.
- [105] I. P. Grant, *Adv. Phys.* **19**, 747 (1970).
- [106] I. P. Grant and H. M. Quiney, *Adv. At. Mol. Phys.* **23**, 37 (1988).
- [107] P. Indelicato, *Phys. Rev. A* **51**, 1132 (1995).
- [108] V. M. Shabaev, *Theor. Math. Phys.* **63**, 588 (1985).
- [109] V. M. Shabaev and A. N. Artemyev, *J. Phys. B: At. Mol. Opt. Phys.* **27**, 1307 (1994).
- [110] V. M. Shabaev, *Phys. Rev. A* **57**, 59 (1998).
- [111] J. Li, C. Nazé, M. Godefroid, S. Fritzsche, G. Gaigalas, P. Indelicato, and P. Jönsson, *Phys. Rev. A* **86**, 022518 (2012).
- [112] J. M. Sampaio, F. Parente, C. Nazé, M. Godefroid, P. Indelicato, and J. P. Marques, *Phys. Scr.* **T156**, 014015 (2013).
- [113] J. P. Santos, J. P. Marques, F. Parente, E. Lindroth, P. Indelicato, and J. P. Desclaux, *J. Phys. B: At. Mol. Phys.* **32**, 2089 (1999).
- [114] J. P. Santos, G. C. Rodrigues, J. P. Marques, F. Parente, J. P. Desclaux, and P. Indelicato, *Eur. Phys. J. D* **37**, 201 (2006).
- [115] M. C. Martins, J. P. Marques, A. M. Costa, J. P. Santos, F. Parente, S. Schlessler, E. O. Le Bigot, and P. Indelicato, *Phys. Rev. A* **80**, 032501 (2009).
- [116] G. Audi, A. H. Wapstra, and C. Thibault, *Nucl. Phys. A* **729**, 337 (2003).
- [117] I. Angeli, *At. Data Nucl. Data Tables* **87**, 185 (2004).
- [118] P. J. Mohr, *Ann. Phys.* **88**, 52 (1974).
- [119] P. J. Mohr, *Phys. Rev. A* **46**, 4421 (1992).
- [120] P. J. Mohr and Y.-K. Kim, *Phys. Rev. A* **45**, 2727 (1992).
- [121] P. Indelicato and P. J. Mohr, *Phys. Rev. A* **46**, 172 (1992).
- [122] E.-O. Le Bigot, P. Indelicato, and P. J. Mohr, *Phys. Rev. A* **64**, 052508 (2001).
- [123] P. J. Mohr and G. Soff, *Phys. Rev. Lett.* **70**, 158 (1993).
- [124] P. Indelicato and E. Lindroth, *Phys. Rev. A* **46**, 2426 (1992).
- [125] P. Indelicato, S. Boucard, and E. Lindroth, *Eur. Phys. J. D* **3**, 29 (1998).
- [126] P. Indelicato and P. J. Mohr, *Hyperfine Interact.* **114**, 147 (1998).
- [127] V. M. Shabaev, I. I. Tupitsyn, and V. A. Yerokhin, *Comput. Phys. Commun.* **189**, 175 (2015).
- [128] P. Indelicato and P. J. Mohr, *Phys. Rev. A* **63**, 052507 (2001).
- [129] S. A. Blundell, *Phys. Rev. A* **47**, 1790 (1993).
- [130] P. Indelicato, F. Parente, and R. Marrus, *Phys. Rev. A* **40**, 3505 (1989).
- [131] P.-O. Löwdin, *Phys. Rev.* **97**, 1474 (1955).
- [132] P. Indelicato, *Hyperfine Interact.* **108**, 39 (1997).
- [133] C. Froese Fischer, *The Hartree-Fock Method for Atoms* (Wiley, New York, 1977).
- [134] O. Gorcex, P. Indelicato, and J. P. Desclaux, *J. Phys. B: At. Mol. Opt. Phys.* **20**, 639 (1987).
- [135] P. Indelicato, *Phys. Rev. Lett.* **77**, 3323 (1996).
- [136] R. D. Deslattes, E. G. Kessler, Jr., P. Indelicato, L. de Billy, E. Lindroth, and J. Anton, *Rev. Mod. Phys.* **75**, 35 (2003).
- [137] G. Howat, T. Åberg, and O. Goscinski, *J. Phys. B: At. Mol. Opt. Phys.* **11**, 1575 (1978).
- [138] M. F. Gu, *Can. J. Phys.* **86**, 675 (2008).
- [139] A. M. Costa, M. C. Martins, F. Parente, J. P. Santos, and P. Indelicato, *At. Data Nucl. Data Tables* **79**, 223 (2001).
- [140] L. Natarajan, *J. Phys. B: At. Mol. Opt. Phys.* **36**, 105 (2003).
- [141] G. W. F. Drake, *Phys. Rev. A* **19**, 1387 (1979).
- [142] W. R. Johnson, D. R. Plante, and J. Sapirstein, in *Advances in Atomic, Molecular and Optical Physics*, Vol. 35, edited by B. Bederson and H. Walther (Addison-Wesley, New York, 1995), pp. 255–329.
- [143] A. Derevianko, I. M. Savukov, W. R. Johnson, and D. R. Plante, *Phys. Rev. A* **58**, 4453 (1998).
- [144] P. Indelicato, V. M. Shabaev, and A. V. Volotka, *Phys. Rev. A* **69**, 062506 (2004).
- [145] R. Si, X. L. Guo, K. Wang, S. Li, J. Yan, C. Y. Chen, T. Brage, and Y. M. Zou, *Astron. Astrophys.* **592**, A141 (2016).
- [146] C. I. Szabo, P. Amaro, M. Guerra, S. Schlessler, A. Gumberidze, J. P. Santos, and P. Indelicato, in *CAARI*, AIP Conf. Proc. No. 1525 (AIP, Fort Worth, 2013), pp. 68–72.
- [147] C. I. Szabo, P. Amaro, M. Guerra, J. P. Santos, A. Gumberidze, J. Attard, and P. Indelicato, *Phys. Scr.* **T156**, 014077 (2013).
- [148] D. R. Plante, W. R. Johnson, and J. Sapirstein, *Phys. Rev. A* **49**, 3519 (1994).
- [149] K. T. Cheng, M. H. Chen, W. R. Johnson, and J. Sapirstein, *Phys. Rev. A* **50**, 247 (1994).
- [150] G. W. Drake, *Can. J. Phys.* **66**, 586 (1988).
- [151] U. I. Safronova, *Phys. Scr.* **23**, 241 (1981).
- [152] W. R. Johnson and J. Sapirstein, *Phys. Rev. A* **46**, R2197(R) (1992).
- [153] A. H. Gabriel, *Mon. Not. R. Astron. Soc.* **160**, 99 (1972).
- [154] R. L. Wasserstein and N. A. Lazar, *The American Statistician* **70**, 129 (2016).
- [155] L. Engstrom and U. Litzen, *J. Phys. B: At. Mol. Opt. Phys.* **28**, 2565 (1995).
- [156] L. Schleinkofer, F. Bell, H. D. Betz, G. Trolman, and J. Rothermel, *Phys. Scr.* **25**, 917 (1982).
- [157] H. D. Dohmann, D. Liesen, and H. Pfeng, *Z. Phys. A: Hadrons Nucl.* **285**, 171 (1978).
- [158] P. Beiersdorfer, M. Bitter, S. von Goeler, and K. W. Hill, *Phys. Rev. A* **40**, 150 (1989).
- [159] C. T. Chantler, D. Paterson, L. T. Hudson, F. G. Serpa, J. D. Gillaspay, and E. Takacs, *Phys. Rev. A* **62**, 042501 (2000).
- [160] J. P. Briand, M. Tavernier, R. Marrus, and J. P. Desclaux, *Phys. Rev. A* **29**, 3143 (1984).
- [161] P. Indelicato, M. Tavernier, J. P. Briand, and D. Liesen, *Z. Phys. D* **2**, 249 (1986).
- [162] J. P. Briand, P. Indelicato, A. Simionovici, V. San Vicente, D. Liesen, and D. D. Dietrich, *Europhys. Lett.* **9**, 225 (1989).
- [163] K. Widmann, P. Beiersdorfer, G. V. Brown, J. R. Crespo López-Urrutia, A. L. Osterheld, K. J. Reed, J. H. Scofield, and S. B. Utter, *AIP Conf. Proc.* **506**, 444 (2000).
- [164] J. P. Briand, P. Chevallier, P. Indelicato, K. P. Ziocck, and D. D. Dietrich, *Phys. Rev. Lett.* **65**, 2761 (1990).
- [165] J. H. Lupton, D. D. Dietrich, C. J. Hailey, R. E. Stewart, and K. P. Ziocck, *Phys. Rev. A* **50**, 2150 (1994).
- [166] V. Decaux, P. Beiersdorfer, S. M. Kahn, and V. L. Jacobs, *Astrophys. J.* **482**, 1076 (1997).

- [167] R. Steinbrügge, S. Bernitt, S. W. Epp, J. K. Rudolph, C. Beilmann, H. Bekker, S. Eberle, A. Müller, O. O. Versolato, H. C. Wille *et al.*, *Phys. Rev. A* **91**, 032502 (2015).
- [168] U. I. Safronova and A. S. Shlyaptseva, *Phys. Scr.* **54**, 254 (1996).
- [169] V. A. Boiko, A. Y. Chugunov, T. G. Ivanova, A. Y. Faenov, I. V. Holin, S. A. Pikuz, A. M. Urnov, L. A. Vainshtein, and U. I. Safronova, *Mon. Not. R. Astron. Soc.* **185**, 305 (1978).
- [170] S. Shuqiang, P. Feng, and J. Gang, *J. Phys. B: At. Mol. Opt. Phys.* **39**, 2087 (2006).